Effect of Aeroelasticity In Tow Tank Strain Gauge Measurements On a NACA 0015 Airfoil

A Thesis Presented to
The Faculty of the College of Engineering and Technology
Ohio University

In Partial Fulfillment
of the Requirements for the Degree
Master of Science

by
Sihao Li

August 1993

Acknowledgement

I would like to express my sincere gratitude to my advisor, Dr. Gary M. Graham, for all his guidance, invaluable suggestions patience and encouragement through the course of this work.

I would also like to give my gratitude to the members of my thesis committee, Dr. M. Khairul Alam and Dr. Larry Snyder, for their patience and time in reviewing my thesis and for their comments and suggestions.

Finally, my special great gratitude to my wife, Huan Yao, for her continual support and encouragement during my study in Ohio University.

Table of Contents

Acknowledgement I
Table of Contents II
Nomenclature IV
Chapter 1 Introduction
1.1 Background 1
1.2 Ohio University Tow Tank 2
1.3 Classical Linear Normal Force Response 5
Chapter 2 Aerodynamics of 2D Airfoil
2.1 Steady Aerodynamic Forces on an Airfoil in an Ideal Fluid 9
2.2 Unsteady Aerodynamic Forces on an Airfoil in an Incompressible Fluid 9
Chapter 3 Aeroelastic Analysis
3.1 Lumped Mass Method 17
3.2 Generalized Displacement Method 19
3.3 System Representation 20
3.4 Natural Frequencies and Mode Shapes of the Structure 22
3.5 Mode superposition Method 23
3.6 Dynamic Model of the Structure 25
3.7 Aeroelastic Loading 28
3.7.1 Sign Convention 28
3.72 Normal Loading 29
3.7.3 Aeroelastic Moments 31
3.8 Nondimensionalization 33
3.9 Input Step 36

3.10 Solution of System Equations 37

Chapter 4 Results and Discussion

4.1 Sensible Force at the Load Cell 41

4.2 Results and Discussion 42

4.2.1 Generalize Coordinates for an Instantaneous Step 42

4.2.2 Comparison with Theoretical Normal Force Response 44

4.2.3 Comparison with Experiment Data 44

4.3 Reduced Frequency and Apparent Mass 47

4.4 Limitations and Further Study 51

Chapter 5 Conclusions 52

Appendix A System Matrices 53

Appendix B Solving of the System Equation 59

Appendix C Partial Fraction of the Solution 60

Appendix D Inverse Laplace Transformation 64

References 66

NOMENCLATURE

$[A_n]$	normal degree of freedom flexibility matrix
$[A_t]$	torsional degree of freedom flexibility matrix
b	semichord of the airfoil
C_N	normal force coefficient
C_{N_0}	initial normal force coefficient
DOF	degree of freedom
$[D_n]$	normal degree of freedom system matrix
$[D_t]$	torsional degree of freedom system matrix
F	normal force
g(t)	torsional degree of freedom generalized coordinates
h	normal displacement
$[K_n]$	normal degree of freedom stiffness matrix
$[K_t]$	torsional degree of freedom stiffness matrix
[J]	mass moment of inertia matrix
M	torsional moment
[M]	mass matrix
N	normal force
NDOF	normal degree of freedom
p(t)	generalized coordinates in rigid body rotation
q(t)	normal degree of freedom generalized coordinates
t	physical time (sec)
T	torsional moment
TDOF	torsional degree of freedom
U	free stream velocity
$\{V_n\}$	displacement vectors in normal degree of freedom
$\{V_t\}$	displacement vectors in torsional degree of freedom

2D	two dimensional
α	angle of attack (deg)
$\Delta\alpha$	a step change in angle of attack
$\{\phi_n\}$	mode shape vector in normal degree of freedom
ϕ_{ni}	the ith element of vector $\{\phi_n\}$
$\{\phi_t\}$	made shape vector in torsional degree of freedom
ϕ_{ti}	the ith element of vector $\{\phi_t\}$
$\Gamma(\tau)$	Wagner's function
ρ	density of fluid
τ	nondimensional time, τ=Ut/b

Chapter One

Introduction

1.1 Background

The normal force response of a 2D NACA 0015 airfoil experiencing small and rapid step changes in angle of attack by rotation about the quarter chord has been measured recently in the Ohio University tow tank [1]. The motivation for these experiments was to study nonlinear airfoil behavior as defined in the theory of nonlinear mathematical modeling for aerodynamic systems [2]. In this theory, nonlinear airfoil behavior is predicted by using indicial response functional method in conjunction with nonlinear superposition. The superposition process can be performed using DuHamel integral [3] by considering the motion of an airfoil to be comprised of a series of small steps. Interesting results have been obtained by using this method [4, 6-9]. Knowledge of the loading for each step, is referred to as the indicial response, and remains a central issue in the model.

Recent experiments in a tow tank at O.U. have involved strain gauge load cell measurements of the transient normal force loading on an airfoil undergoing a step change in angle of attack of approximately $\Delta\alpha=+1^\circ$ at a reduced pitch rate ($\dot{\alpha}b/U$, b=semichord) near 0.3. The angle of attack before the step onset (α_0) was steady and was varied over the range $2^\circ < \alpha_0 < 60^\circ$ In these experiments the test rig experiences high levels of inertial, as well as aerodynamic loading due to the rapid starting and stopping required to impart the step. Therefore, an important issue is the degree to which aeroelastic reactions deform the structure and thereby influence the output of the strain gauge bridge. Knowledge of these reactions is essential in comparing these strain gauge data with classical indicial responses such as Wagner's function [10]. The present analysis is an effort to extract the pure aerodynamic part from the output data of the strain gauge bridge including aeroelastic effects. The present study describes an aeroelastic model of the O.U. tow tank load cell/airfoil test rig. The model is based on the mode superposition method for structural systems and classical linear airfoil theory.

1.2 Ohio University Tow Tank

A schematic of the O.U. tow tank is shown in Figure 1.1. The facility consists of a large tank with a six inch chord NACA 0015 airfoil suspended vertically in the water with a submerged length of 42.0 inches. The tank is 30 feet long, 12 feet wide and 4 feet deep. A carriage moves in translation along roller bearings fixed to I-beams spanning the tank at a speed of 2 ft/s, giving a Reynolds number near 95,000. The airfoil is driven in rotation via a drive shaft fixed to the airfoil quarter chord at one end, and coupled to a 3.5 hp stepper motor/gear box apparatus at the other end. Figure 1.2 is a schematic showing details of the drive shaft and airfoil. Shown here are dimensions in inches, and a numbering scheme (1 through 17) defined for the purpose of discretizing the mass of the structure which will be discussed in detail in a latter section. The drive shaft has several variations in cross section over the length of the shaft which must be considered in modeling the aeroelastic response of

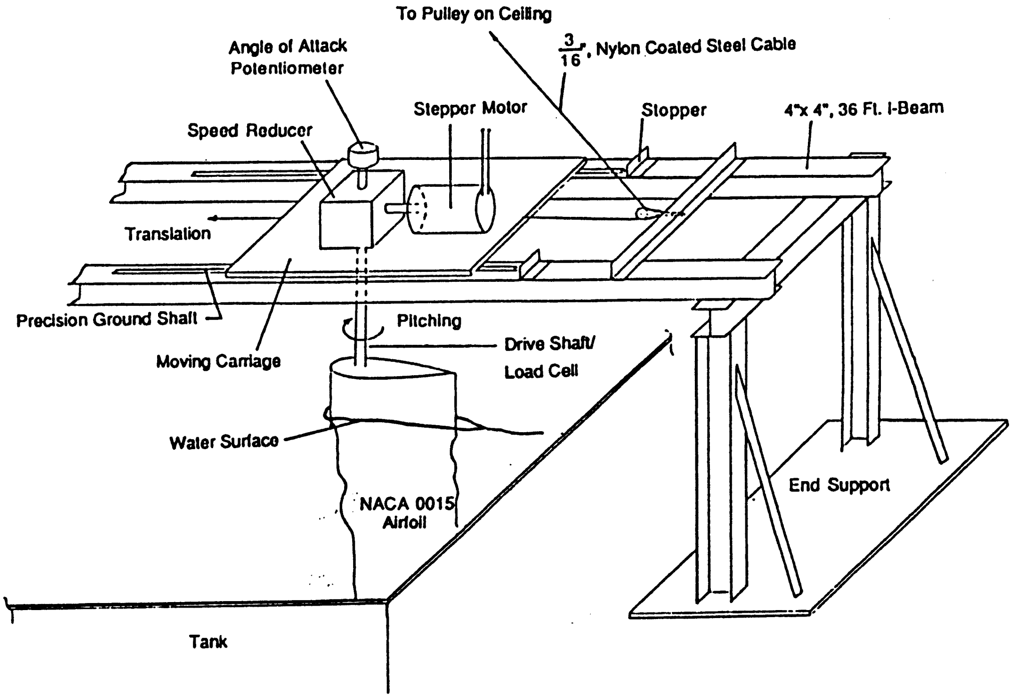

Figure 1.1 Ohio University Tow Tank Facility

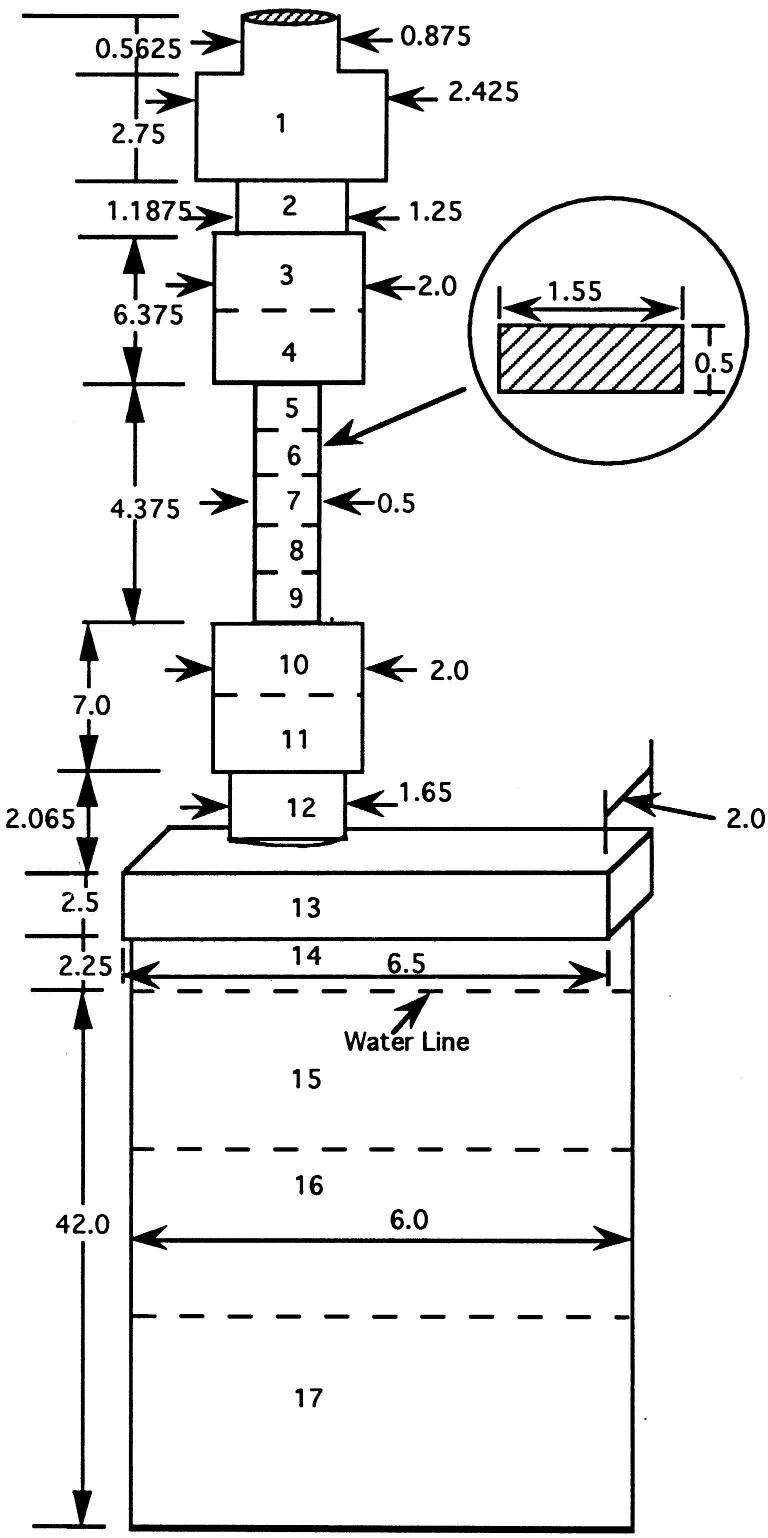

Figure 1.2 Details of the Drive Shaft and Airfoil
(Dimensions are in inches. Drawing is not to scale.)

the structure. Near the middle of the drive shaft is a machined rectangular section upon which strain gauges are mounted. The load cell is discretized into mass elements 5 through 9. The strain gauge circuit is electrically compensated to be sensitive to chord normal forces only. The upper most mass element 1 is made of steel while all other parts are aluminum. The mass of the airfoil per unit length is measured to be 0.1598 lbm/in. The moment of inertia of the airfoil about the quarter chord and polar moment of inertia of the airfoil about the pitch axis are calculated to be 0.12 in^4 and 5.39 in^4 respectively.

The center of mass of the airfoil is calculated to be located 1.27 inches aft of the pitch axis which is at the quarter chord. Following material properties are taken for later calculation: Young's modulus of elasticity of steel: 30×10^6 psi, Young's modulus of elasticity of aluminum: 7.0×10^6 psi, density of steel: 0.282 lbm/in^3, density of aluminum: 0.098 lbm/in^3.

1.3 Classical Linear Normal Force Response

In an incompressible flow, the theoretical linear normal force coefficient response of a flat plate airfoil given an instantaneous step change in angle of attack by rotation about the quarter chord can be shown to be [3,4]:

$$C_N(t)=C_{N_0}+\pi\Delta\alpha[\delta(t-0)+\frac{1}{2}\delta'(t-0)]+2\pi\Delta\alpha[1-0.157e^{-.0455t}-0.235e^{-.3t}] \tag{1.1}$$

where C_{N_0} is the initial normal force, $\Delta\alpha$ is the step amplitude, and δ' is the time derivative of the Dirac delta function δ[12]. The first two terms in brackets in Equation 1.1 are generalized functions [12] which describe the noncirculatory component of the loading, while the last group of terms is the circulatory component. The exponential terms arise from a two pole curve fit to Wagner's function [3,10]. Equation 1.1 is referred to as the indicial response (actually, the derivative of Eqn. 1.1 w.r.t. α) and is important in the convolution integral formulation for the loading on an airfoil in arbitrary motion.

Transient normal force responses of a NACA 0015 airfoil undergoing rapid small amplitude changes in angle of attack by rotation have been measured in the O.U. tow tank. Figure 1.3a shows angle of attack data for a typical run (small spikes are electrical noise). The onset angle is 2.09° and the step amplitude is approximately +1.3°. The motion resembles, to a reasonable approximation, a small amplitude ramp at a reduced rate near 0.3. Figure 1.3b is a comparison of the experimental normal force response to Equation 1.1. To facilitate the comparison, the coefficient 2π (for a flat plate airfoil) on the circulatory part in Equation 1.1 has been replaced by the experimentally measured local static normal force curve slope (for the present NACA 0015) measured at the onset angle in an independent test [1]. This substitution is necessary for the response of Equation 1.1 to approach the same steady state response as the experimental response. The analysis which follows is designed to study the effects of aeroelasticity on the comparison of the experimental and theoretical responses of Figure 1.3b.

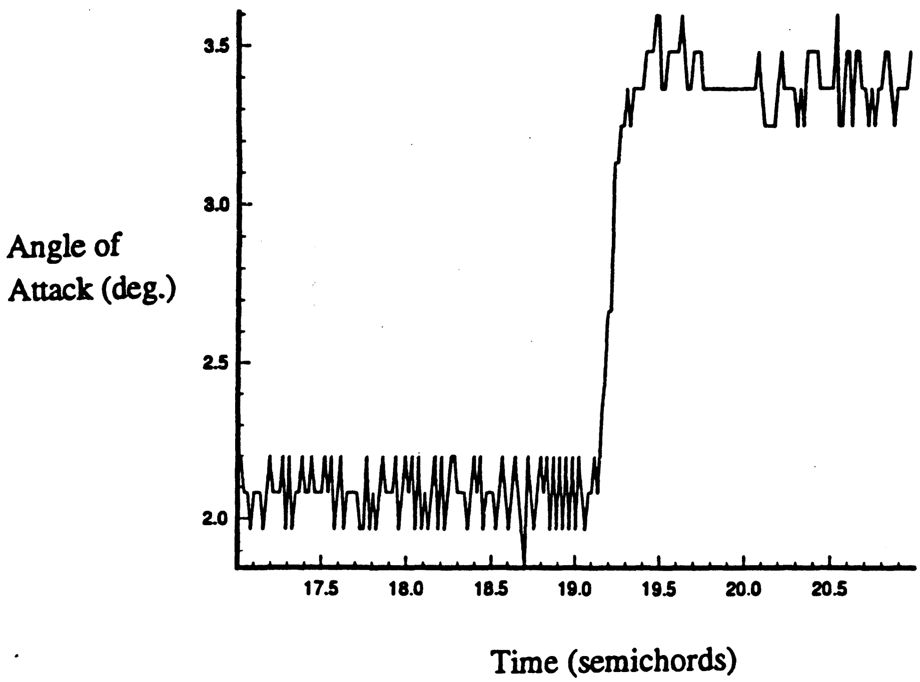

Figure 1.3a Angle of Attack Data for Indicial Response Test

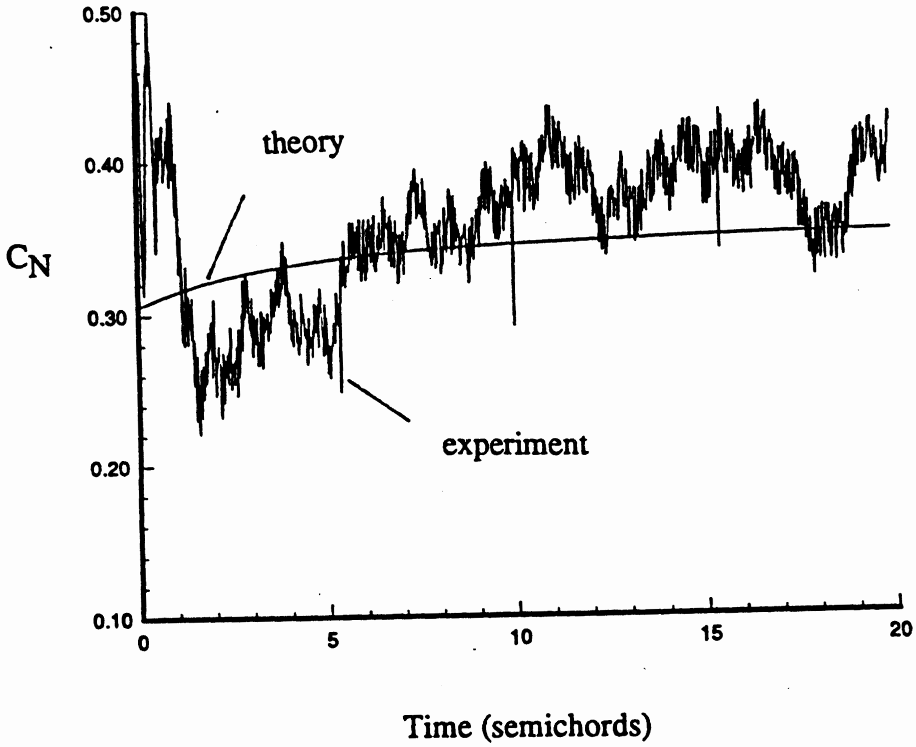

Figure 1.3b Comparison of Normal Force Coefficient Data with Theoretical Response.

Chapter Two

Aerodynamic of 2D Airfoil

2.1 Steady Aerodynamic Forces on an Airfoil in an Ideal Fluid

In the theory of potential flow, the lift force acting on the airfoil is determined by the circulation around the airfoil. This circulation arises from the Kutta condition which may be stated as follows: for bodies with sharp trailing edges which are at small angles of attack to the free stream, the flow will adjust itself in such a way that the rear stagnation point coincides with the trailing edge. The normal force on a flat-plate airfoil is given by [13]:

$$N = 2\pi\rho U^2 b \sin\alpha \tag{2.1}$$

where N is the normal force, ρ is the density of the fluid, U is the velocity of free stream, b is semichord length, and α is the angle of attack. Then the value of the lift coefficient ($C_N = N/\rho U^2 bl$) for the flat-plate airfoil is:

$$C_N = 2\pi \sin\alpha \tag{2.2}$$

2.2 Unsteady Aerodynamic Forces on an Airfoil in an Incompressible Fluid

The unsteady aerodynamic force acting on a thin airfoil in unsteady motion in a two-dimensional incompressible fluid was obtained by Wagner, Kussner, Von Karman and Sears, and others. Let the chord of the airfoil be 2b, and the angle of attack (assumed infinitesimal) be α. Consider the increase of circulation around the airfoil which starts impulsively from rest to a uniform velocity U. Let the impulsive motion occur at the origin when $\tau=0$. The vertical velocity component of the fluid, the so-called upwash, is $w=U\sin\alpha$ on the airfoil, since the flow must be tangent to the airfoil. Based on the physical assumption that the velocity at the trailing edge must be finite, the lift due to circulation acting on a strip of unit span can be derived as a function of time [11]:

$$N_{cir}=2\pi b\rho U w\Gamma(\tau) \tag{2.3}$$

where $\tau=Ut/b$ is the nondimensional time based on semichord. Subscript cir denotes the lift arises from circulation. The function $\Gamma(\tau)$ is called Wagner's function. The exact form of $\Gamma(\tau)$ is [3]:

$$\Gamma(\tau)=1-\int_0^{\infty}\left[(K_0-K_1)^2+\pi^2(I_0+I_1)^2\right]^{-1}e^{-x\tau}x^{-2}dx \tag{2.4}$$

where K_0, K_1, I_0, I_1 are modified Bessel functions of the second and first kind, respectively, with argument x implied. A two pole curve fit to Wagner's function is given by:

$$\Gamma(\tau)=1-0.157e^{-0.0455\tau}-0.335e^{-0.3\tau} \tag{2.5}$$

Figure 2.1 shows the Wagner function. It is seen that half of the final lift is assumed at once and that the lift approaches asymptotically its steady-state value $2\pi b\rho Uw$ when τ goes to infinity. The center of pressure of this lift (due to circulation) is at the quarter-chord point behind the leading edge.

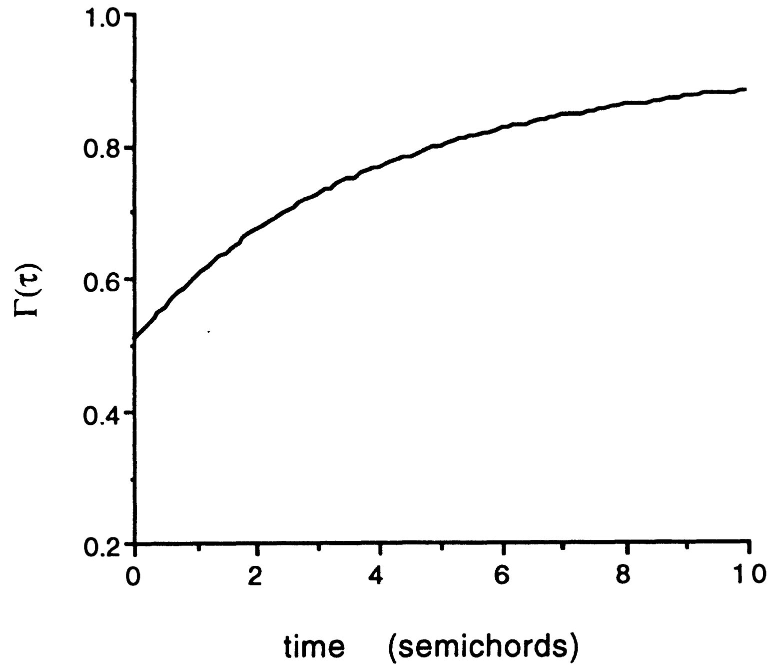

Figure 2.1 Wagner Function

Now we consider a more general type of motion. Let the airfoil have two degrees of freedom: a vertical (normal) translation h measured at the pitch axis, called plunge, positive upward, and a rotation α, called pitching, positive nose up, about an axis located at a distance $a_h b$ from the mid-chord point, a_h being positive toward the trailing edge (Figure 2.2). The flow is assumed to be two dimensional, h and

α are infinitesimal, and the free flow speed U is a constant. In this case part of the lift arises from circulation due to boundary vorticity, and part from noncirculatory flow due to a source-sink distribution origin.

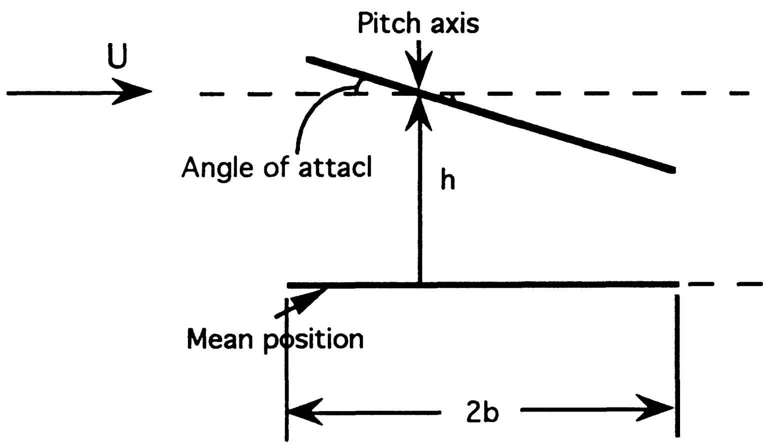

Figure 2.2 Notations.

Wagner's function gives the increase of circulation around the airfoil due to a sudden increase of downwash due to plunge. For a general motion having two degrees of freedom h and the downwash over the airfoil is not uniform. In the theory of harmonic oscillation airfoils, it can be shown that for plunging and pitching oscillations the circulation about the airfoil is determined by the downwash velocity at the 3/4-chord point from the leading edge of the airfoil (see reference 11, Chapter 13). By a reciprocal relation between the harmonic oscillations and the response to unit-step functions (reference 11, Chapter 15), and the principle of superposition, this result holds also for arbitrary plunging and pitching motions. Therefore, if we replace w in Equation 2.3 by the increment of downwash at the 3/4-chord point, the circulatory lift can be obtained.

The downwash at the 3/4-chord point due to h and α degrees of freedom comes from three sources: (1) a uniform downwash due to a pitching angle α, $w=U\sin\alpha$, (2) a uniform downwash due to vertical translation $\dot{h}$, which can be written as $-dh/dt=-(dh/d\tau)(dt/d\tau)=-Uh'/b$ where a prime denotes a differentiation with respect to the nondimensional time τ, and a dot denotes a differentiation with respect to physical time t, (3) a nonuniform downwash due to α', its value at the 3/4-chord being $(0.5-a_h)b(d\alpha/dt)$ or $(0,5-a_h)U\alpha'$. Summing up, we get:

$$w(\tau) = U\sin\alpha - \frac{U}{b}h'(\tau) + (\frac{1}{2} - a_h)U\alpha'(\tau) \tag{2.6}$$

In the time interval $(\tau_0, \tau_0+d\tau_0)$, the downwash $w(\tau_0)$ increases by an amount $dw(\tau_0)$. If $d\tau_0$ is sufficiently small, this can be regarded as an impulsive increment and the corresponding circulatory lift per unit span is:

$$dN_{cir}=2\pi b\rho U\Gamma(\tau-\tau_0)\frac{dw(\tau_0)}{d\tau_0}d\tau_0 \tag{2.7}$$

When the w is small, the principle of superposition holds. Thus we may apply DuHamel's integral to get the circulatory lift per unit span for arbitrary time history of w:

$$N_{cir}(\tau)=2\pi b\rho U\int_{-\infty}^{\tau}\Gamma(\tau-\tau_0)\frac{dw(\tau_0)}{d\tau_0}d\tau_0 \tag{2.8}$$

where the lower limit is taken as minus infinity, meaning before the very beginning of motion. If the motion starts at time $\tau=0$, and $w=0$ for $\tau<0$, Equation 2.8 reduces to:

$$N_{cir}(\tau)=2\pi b\rho U[w_0\Gamma(\tau)+\int_0^{\tau}\Gamma(\tau-\tau_0)\frac{dw(\tau_0)}{d\tau_0}d\tau_0] \tag{2.9}$$

where w_0 is the limiting value of w when τ approaches zero from the positive side. Combine Equations 2.6 and 2.8:

$$N_{cir}(\tau)=2\pi b\rho U\{w_0\Gamma(\tau)+U\int_0^{\tau}\Gamma(\tau-\tau_0)[\alpha'(\tau_0)-\frac{1}{b}h''(\tau_0)+(\frac{1}{2}-a_h)\alpha''(\tau_0)]d\tau_0\} \tag{2.10}$$

where superscript prime denotes differentiation with respect to the nondimensional time τ, and dot denotes differentiation with respect to the physical time t. The center of pressure of this circulatory lift is at the quarter-chord point behind the leading edge.

The derivation of the noncirculatory lift and moment is presented in reference [11]. The results are as follows:

1. The apparent mass term which is equal to the apparent mass $\pi\rho b^2$ times the vertical acceleration at the mid-chord point:

$$N_{app}=-\pi\rho b^2(\ddot{h}+a_h b\ddot{\alpha})=-\pi\rho U^2(h''+a_h b\alpha'') \tag{2.11}$$

The center of pressure of this force is at the mid-chord point.

2. The centrifugal force which is equal to the apparent mass times $U\dot{\alpha}$:

$$N_{cen}=\pi\rho b^2 U\dot{\alpha}=\pi\rho b U^2\alpha' \tag{2.12}$$

The center of pressure of this centrifugal force is at the 3/4-chord point behind the leading edge.

3. A nose down couple which is equal to the apparent moment of inertia $\pi\rho b^2(b^2/8)$ times the angular acceleration:

$$M_a=-\frac{\pi\rho b^4}{8}\ddot{\alpha}=-\frac{\pi\rho b^2U^2}{8}\alpha'' \tag{2.13}$$

As a result, the total lift per unit span is:

$$N=N_{cir}+N_{app}+N_{cen} \tag{2.14}$$

The total moment per unit span about the elastic axis is:

$$M=(\frac{1}{2}+a_h)bN_{cir}+a_hbN_{app}-(\frac{1}{2}-a_h)bN_{cen}+M_a \tag{2.15}$$

Equations 2.14 and 2.15 give the total lift and moment when the airfoil undergoes a motion with two degrees of freedom: bending and pitching. They are valid only for incompressible fluid and small angle of attack.

Chapter Three

Aeroelastic Analysis

The present analysis is based on a combination of the mode superposition method [14] for dynamic structural response to forced vibration, and linear airfoil theory formulated in terms of the convolution integral representation of the loading on an airfoil in arbitrary motion.

3.1 Lumped Mass Method

In the dynamic system of Fig. 3.1, the analysis obviously is greatly complicated by the fact that the inertia forces result from structural displacements which in turn are influenced by the magnitudes of inertia forces. This closed cycle of cause and effect can be attacked directly only by formulating the problem in terms of differential equations. Furthermore, because the mass of the beam is distributed continuously along its length, the displacements and accelerations must be defined for each point along the axis if the inertia forces are to be completely defined. In this case, the analysis must be formulated in terms of partial differential equations because the position along the span as well as the time must be taken as independent variables.

On the other hand, if the mass of the beam were concentrated on a series of discrete points or lumps, as shown in Fig. 3.2, the analytical problem would be greatly simplified because inertia

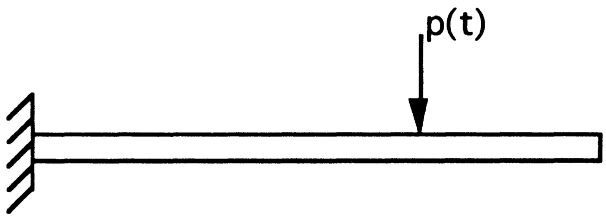

Fig. 3.1 A cantilever beam

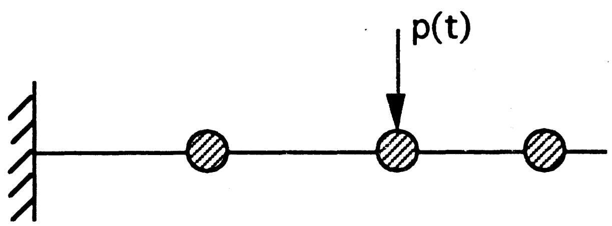

Fig. 3.2 Lumped-mass idealization of a cantilever beam

forces could be developed only at these mass points. In this case it is necessary to define the displacements and accelerations only at these discrete points.

The number of displacement components that must be considered in order to represent the effects of all significant inertia forces of a structure may be termed the number of dynamic degrees of freedom of the structure. For example, if the system of Fig. 4b were constrained so that the three mass points could move only in a vertical direction, this would be called a three-degree-of-freedom (3 DOF) system. On the other hand, if these masses were not concentrated in points but had finite rotational inertia, the rotational displacements of the three points would also have to be considered and the system would have 6 DOF.

3.2 Generalized Displacement Method

In the case where the mass of the system is quite uniformly distributed throughout, however, an alternative approach to limiting the degrees of freedom may be preferable. This procedure is based on the assumption that the deflected shape of the structure can be expressed as the sum of a series of specified displacement patterns, these patterns then become the displacement coordinates of the structure. In general, any shapes $f_n(x)$ which are compatible with the prescribed geometric-support conditions and which maintain the necessary continuity of internal displacements may be used as the displacement patterns. Thus a generalized expression for the displacements of any one-dimensional structure might be written as:

$$v(x) = \sum_n z_n f_n(x) \tag{3.1}$$

For any assumed set of displacement functions $f_n(x)$, the resulting shape of the structure depends upon the amplitude terms z_n, which is referred to as generalized coordinates. The number of assumed shape patterns represents the number of DOF considered in this form of idealization.

3.3 System Representation

As illustrated in Fig. 1.2, the structure under consideration has been discretized into 17 mass elements that are considered to be concentrated at the centroid of each element. The lowest three masses (15-17) represent the submerged portion of the airfoil, and masses 5 through 9 correspond to the rectangular cross section load cell. Masses are concentrated on the load cell to obtain good resolution of the deformation there, from which the "sensible" strain may be computed from the beam curvature.

Both normal and torsional vibration degrees of freedom are considered here, because the pitch axis does not coincide with the center of mass of the lower part of the structure (mass elements 13-17). For the normal degree of freedom (NDOF), each mass element communicates with neighboring masses through NDOF stiffness elements. For the torsional degree of freedom (TDOF), the structure is discretized in the same way as the NDOF for elements 1 through 12, however elements 13 through 17 are lumped into a single inertia element giving a total of 13 inertia elements. The reduction in elements in the TDOF is based on the fact that the torsional stiffness of both the mounting block (element 13) and the airfoil are much larger than the drive shaft, and consequently the mounting block and entire airfoil experience nearly the same TDOF deflection.

The resulting discretized structure may be described mathematically in terms of a diagonal mass matrix [M] (17x17), a symmetric NDOF flexibility 17x17 matrix $[A_n]$ (17x17), a diagonal polar mass moment of inertia matrix [J] (13x13), and a symmetric TDOF flexibility matrix $[A_t]$ (13x3). Matrix [M] and [J] can be calculated by knowing the dimensions and material properties of each element. The values of [M] and [J] are given in appendix A.

The definition of flexibility influence coefficient $A_{ni,j}$ and $A_{ti,j}$ are as follows

$A_{ni,j}$ = deflection of mass i due to a unit force applied at mass j (3.2a)

$A_{ti,j}$ = angular rotation of polar inertia i due to a unit torque applied to polar inertia j (3.2b)

Virtue work method [15] is employed here to calculate $A_{ni,j}$ according to it's definition. $A_{ti,j}$ is computed from elementary mechanics for shafts in torsion. Sample calculations and the values of $[A_n]$ and $[A_t]$ are presented on Appendix A.

The NDOF stiffness matrix $[K_n]$ and TDOF stiffness matrix $[K_t]$ are computed by inverting $[A_n]$ and $[A_t]$. IMSL subroutines are used for the inverting of $[A_n]$ and $[A_t]$, and the results are checked by using commercial software Matlab [16] on a Sun workstation.

3.4 Natural Frequencies and Mode Shapes of the Structure

The system matrices above have been used to solve the eigenvalue, or free vibration, problem to compute the natural frequencies and mode shape vectors of the structure. This has been done in the usual way by assuming that free-vibration motion is simple harmonic, which results in the frequency equations

$$|\lambda_n[I] - [D_n]| = 0 \qquad (3.3a)$$

$$|\lambda_t[I] - [D_t]| = 0 \qquad (3.3b)$$

where the λ's are eigen values of the system matrix which are equal to the inverse square of the natural frequencies given by $\lambda_n = 1/\omega_n^2$, $\lambda_t = 1/\omega_t^2$, and [I] is identity matrix. $[D_n]$ and $[D_t]$ are system matrices given by $[D_n] = [A_n][M]$ and $[D_t] = [A_t][J]$. The problem to find the natural frequencies and mode shapes of the structure is now reduced to find the eigenvalues and eigenvectors of system matrix $[D_n]$ and $[D_t]$. This has been done by using IMSL subroutines and the results are checked by commercial software Matlab [16] on Sun workstation. The most significant results is the lowest natural frequency (or the largest eigenvalue) and its corresponding mode shape (eigenvector). The values of the two lowest natural frequencies for the NDOF and TDOF, respectively, are ω_n = 7.74 hz and ω_t = 97.38 hz and their respective mode shapes are:

$$\{\phi_n\}_1 = \{.0017,\ .0043,\ .0115,\ .0246,\ .0343,\ .0394,\ .0454,\ .0523,\ .0599,\ .0813,\ .118,\ .148,\ .174,\ .203,\ .332,\ .641,\ 1.0\}$$

(3.4a)

$$\{\phi_t\}_1=\{.0317, .0567, .0897, .109, .200, .363, .526, .688, .851, .943, .964, .986, 1.0\} \quad (3.4b)$$

where subscript 1 denotes the first or fundamental mode shape. $\{\phi_n\}_1$ is graphed in Fig. 3.3. In later section we will see that it is necessary to extend $\{\phi_t\}$ from a 13x1 vector to a 17x1 vector to make $\{\phi_t\}$ mathematically compatible with the 17x1 vector $\{\phi_n\}$ in certain matrix multiplications. This extension is realized by setting the values of elements 14 through 17 of vector $\{\phi_t\}$ the same as the value of element 13 of vector $\{\phi_t\}$ as shown in Equation (3.4c).

$$\{\phi_t\}_1=\{.0317, .0567, .0897, .109, .200, .363, .526, .688, .851, .943, .964, .986, 1.0, 1.0, 1.0, 1.0, 1.0\} \quad (3.4c)$$

The extension is based on the fact that the torsional stiffness of elements 13 through 17 is much larger than that of elements 1 through 12, as such the element 13 through 17 will undergo almost the same torsional deflection in reality.

3.5 Mode Superposition Method

Mode superposition method [14] is the combination of the lumped mass method and generalized displacement method described in section 3.1 and 3.2, wherein the displacement patterns in Equation 3.1 is replaced by mode-shape vectors $\{\phi_n\}_i$ and $\{\phi_t\}_i$. Hence, the

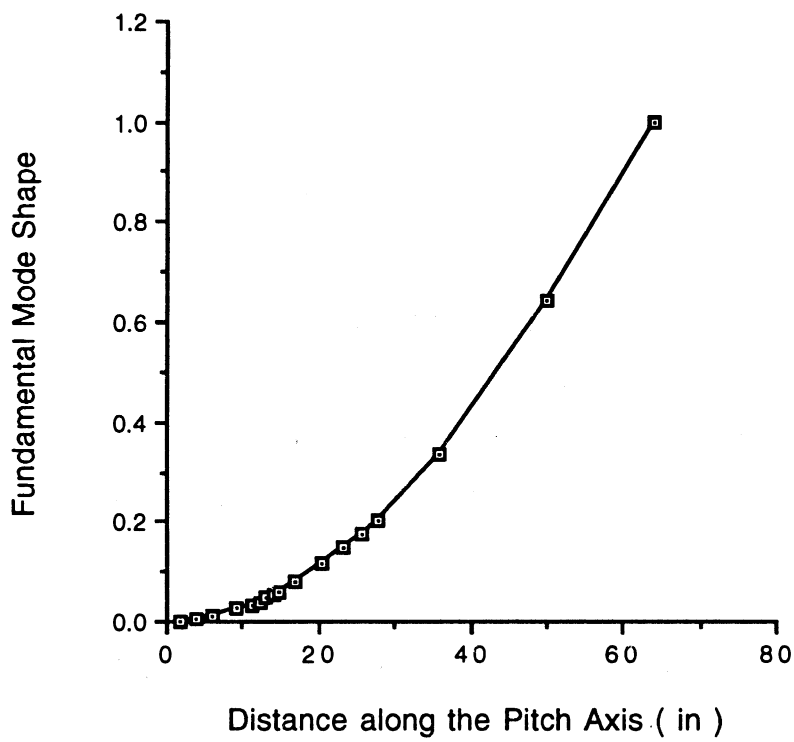

Figure 3.3 Fundamental Mode Shape of NDOF

displacement vectors of NDOF and TDOF can be expressed as

$$\{V_n\} = \sum_{i=1}^{17} \{\phi_n\}_i q_i \tag{3.5a}$$

$$\{V_t\} = \sum_{i=1}^{13} \{\phi_t\}_i g_i \tag{3.5b}$$

where $\{V_n\}$ and $\{V_t\}$ are displacement vectors of NDOF and TDOF respectively with $\{V_n\}_i$ and $\{V_t\}_i$ represent the displacements of the ith element. The mode shapes constitute independent displacement patterns, and the amplitudes q_i and g_i are served as generalized coordinates to express any form of displacement. The reason to use mode shapes as the displacement patterns is because their orthogonality properties [14] and because they describe the displacements efficiently so that good approximations can be made with few terms.

Equations 3.5a and 3.5b can be written in matrix form:

$$\{V_n\} = [\phi_n]\{q\} \tag{3.6a}$$

$$\{V_t\} = [\phi_t]\{g\} \tag{3.6b}$$

where $[\phi_n]$ and $[\phi_t]$ are 17x17 matrix and 13x13 matrix respectively whose ith columns are the ith mode shape vectors of NDOF and TDOF.

3.6 Dynamic Model of the Structure

With d'Alembert's principle [13], the equations of dynamic equilibrium of the structure can be written:

$$[M]\frac{d^2\{V_n\}}{dt^2} + [K_n]\{V_n\} = \{F\} \tag{3.6a}$$

$$[J]\frac{d^2\{V_t\}}{dt^2} + [K_t]\{V_t\} = \{T\} \tag{3.6b}$$

where $[K_n]$ and $[K_t]$ are stiffness matrices of NDOF and TDOF respectively, and $\{F\}$ and $\{T\}$ are loading vectors of NDOF and TDOF on the structure respectively. The damping of the structure is neglected.

Combining Equations 3.5 and 3.6 yields:

$$[M][\phi_n]\{\ddot{q}\} + [K_n][\phi_n]\{q\} = \{F\} \tag{3.7a}$$

$$[J][\phi_t]\{\ddot{g}\} + [K_t][\phi_t]\{g\} = \{T\} \tag{3.7b}$$

where the double dot means the second derivative with respect to physical time.

There are 30 unknown generalized coordinates in Equations 3.7a-b. The present analysis, however, considers only the lowest (fundamental) frequency NDOF vibration mode and lowest TDOF mode and, as such, there is in reality no mode superposition. The justification for neglecting higher frequencies is based on the observation that oscilloscope traces of the strain gauge output, when the structure is excited with no water in the tank, indicate that the fundamental frequencies are dominant. Inclusion of higher frequencies increases the complexity of the algebra.

For modeling the solid body rotation of the test rig, a rotation DOF (RDOF) is introduced. The RDOF is used to simulate the change in angle of attack of the structure due to the rotation imparted by the stepper motor. Notice that the TDOF as defined above simulates only torsional deformations relative to the top of the structure. Now the total deflection of the structure can be written as

$$\{V_n\} = \{\phi_n\}_1 q(t) \tag{3.8a}$$

$$\{V_t\} = \{\phi_t\}_1 g(t) \tag{3.8b}$$

$$\alpha = p(t) \tag{3.8c}$$

where q and g are actually the first element of vector $\{q\}$ and $\{g\}$ respectively, and $\{\phi_n\}_1$ and $\{\phi_t\}_1$ are fundamental mode shapes. The scaler RDOF motion variable α is simply the magnitude of the nominal angle of attack as the structure is pitched and thus is a known variable for a prescribed motion. Actually the vibration of the whole structure is induced by the instantaneous input torque of the stepper motor (in other words a sudden change in α).

In the present analysis, the coordinate p allows the structure to undergo solid body rotation while the coordinates q and g measure deflections relative to the instantaneous position of the top of the structure (where the NDOF and TDOF deflections are zero).

Premultiplying 3.7a by $\{\phi_n\}_1^T$, to make use of the orthogonal properties of mode shapes [14] ($\{\phi_n\}_m^T[M]\{\phi_n\}_n = 0$, and $\{\phi_n\}_m^T[K_n]\{\phi_n\}_n = 0$, when m is not equal to n), we obtain:

$$M\ddot{q} + K_n q = F \tag{3.9a}$$

where M $(=\{\phi_n\}_1{}^T[M]\{\phi_n\}_1)$ is the generalized mass, K_n $(=\{\phi_n\}_1{}^T[K_n]\{\phi_n\}_1)$ is the generalized NDOF stiffness, F $(=\{\phi_n\}_1{}^T\{F\})$ is the generalized force, and q is the same as in Equation 3.8a.

Similarly, premultiplying Equation 3.7b by $\{\phi_t\}_1{}^T$ yields:

$$J\ddot{g} + K_t g = T \tag{3.9b}$$

where J $(=\{\phi_t\}_1{}^T[J]\{\phi_t\}_1)$ is the generalized polar mass moment of inertia about the pitch axis, K_t $(=\{\phi_t\}_1{}^T[K_t]\{\phi_t\}_1)$ is the generalized TDOF stiffness, T $(=\{\phi_t\}_1{}^T\{T\})$ is the generalized aeroelastic moment, and g is the same as in Equation 3.8b. Because only one mode shape for each of NDOF and TDOF is considered in present analysis, the subscript 1 will be omitted in later discussion.

Before solving Equations 3.9a-b, it is necessary to formulate the loading terms on the right hand side of Equations 3.9a-b.

3.7 Aeroelastic Loading

3.7.1 Sign Convention

The sign conventions for the normal force and moment are defined such that a positive angle of attack (in the static sense) produces a positive normal force, while a positive moment produces a nose-up torque. For generalized coordinates, q, g, and p, the sign convention is as follows: a positive normal force tends to produce a positive change in q and it's time derivatives (note this is the reverse of the usual definition used for airfoils in which the NDOF coordinate i.e. plunge is measured in the opposite direction from the normal force); a positive moment tends to produce a positive change in g.

3.7.2 Normal loading

The normal force acting on the structure is composed of three parts: a) rigid body force vector, $\{F_R\}$, which is caused by the step change of angle of attack of the airfoil, b) aeroelastic force vector, $\{F_A\}$, caused by time dependent elastic deflections along the span of the airfoil, and c) inertial force vector, $\{F_I\}$, arise from the fact that the centroids of masses 13 through 17 do not coincide with the pitch axis, therefore the angular acceleration about the pitch axis produces an inertial normal force which acts at the centroid.

The rigid body force vector is the ideal aerodynamic loading response to a step change in angle of attack due to rotation about the quarter chord. These aerodynamic forces are acting only upon the submerged part of the airfoil represented by masses 15,16, and 17 in Figure 1.2. According to Equation 2.14, the aerodynamic force due to rigid body rotation p(t) is given by

$$F_{Ri} = 0\,, \qquad \text{for } i=1,2,\ldots,14$$

$$F_{Ri} = \pi l_i \rho b U^2 \{\frac{1}{2}\ddot{p}(t)+\dot{p}(t)+2\int_0^t \Gamma(t-\tau)[\dot{p}(t)+\ddot{p}(t)]d\tau\} \qquad \text{for } i=15,16,17$$

$$(3.10)$$

where ρ is the density of water, l_i is the length of airfoil element i (note that $l_{15}=l_{16}=l_{17}=4.667$ in), b is the semichord length of the airfoil, U is the velocity of free stream, and $\Gamma(t-\tau)$ is Wagner's function given by Equation 2.5. Notice that $\{F_R\}$ is not a function of the generalized coordinates q and g since in the ideal response the loading is given by (rigid body motion) 2D airfoil theory alone.

For pitch axis at the quarter chord, the aeroelastic force vector, $\{F_A\}$, which is acting upon the submerged part of the airfoil again, is also based on the convolution integral formulation for an airfoil in arbitrary motion [3,11]. According to Equation 2.14 the aerodynamic force due to NDOF and TDOF motion q(t) and g(t) is given by

$$F_{Ai} = 0 \,, \qquad \text{for } i=1,2,\ldots,14$$

$$F_{Ai}(t) = \pi l_i \rho b U^2\{-\frac{1}{b}\phi_{ni}\ddot{q}(t)+\frac{1}{2}\phi_{ti}\ddot{g}(t)+\phi_{ti}\dot{g} + 2\int_0^t \Gamma(t-\tau)[\phi_{ti}\dot{g}(t)+\phi_{ti}\ddot{g}(t)-\frac{1}{b}\phi_{ni}\ddot{q}(t)]d\tau\} \,, \qquad \text{for } i=15,16,17 \tag{3.11}$$

where ϕ_{ni} is the value of the NDOF mode shape $\{\phi_n\}$ at element i, and ϕ_{ti} is the value of the TDOF mode shape.$\{\phi_t\}$ at element i. Notice that it is necessary now to extend $\{\phi_t\}$ from 13x1 vector to 17x1 vector as described in section 3.4. The negative sign on the NDOF term comes from the sign convention adopted.

Because the centroids of mass 13 through 17 do not coincide with the pitch axis, the angular acceleration about the pitch axis produces an inertial normal force at the centroid of each mass. Moreover, due to the fact that the centroid of mass 13 through 17 is behind the axis, a nose-up acceleration will produce a positive initial force, hence,

$$F_{Ii} = 0\,, \qquad \text{for } i=1,2,\ldots,12$$
$$F_{Ii}(t) = m_i r_i[\phi_{ti}\ddot{g}(t)+\ddot{p}(t)]\,, \qquad \text{for } i=13,14,\ldots,17 \tag{3.12}$$

where m_i is the mass of element i and r_i is the distance from pitch axis to the centroid of element i.

3.7.3 Aeroelastic Moments

The TDOF system has been discretized into 13 elements in solving the eigenvalue problem and calculating the generalized inertia and stiffness of the TDOF. However, due to the coupling of NDOF and TDOF there is difficulty in the analysis of aeroelastic moments if we still use 13 elements. To overcome this difficulty, the mode shape vector $\{\phi_t\}$ is now extended from a 13x1 vector to the 17x1 vector and the moment vector {T} is also extended to 17x1. This extension does not affect the results for the TDOF generalized inertia and generalized stiffness computed in the 13 element representation.

The moment acting on the structure is also composed of three parts: a) rigid body moment vector, $\{T_R\}$, which is caused by the step change of angle of attack of the airfoil, b) aeroelastic moment vector, $\{T_A\}$, caused by time dependent elastic deflections along the span of the airfoil, and c) inertial moment vector, $\{T_I\}$. The rigid body moment and the aeroelastic moment act only on the submerged part of the airfoil. The expressions for these moments are simplified by the fact that the circulatory normal force acts at the quarter chord (for a flat plate airfoil) giving a zero moment arm in the present study. For a NACA 0015 airfoil the circulatory normal force (at $Re \sim 10^5$) acts within 2% fraction of chord from the quarter chord and on this basis has been neglected. According to Equation 2.15 the rigid body moment for rotation about the quarter chord is given by

$$T_{Ri} = 0 \,, \qquad \text{for } i=1,2,\ldots,14$$

$$T_{Ri}(t) = -\pi l_i \rho b^2 U^2 [\frac{3}{8}\ddot{p}(t) + \dot{p}(t)] \,, \qquad \text{for } i=15,16,17$$

(3.13)

The aeroelastic moment vector due to NDOF and TDOF motion q(t) and g(t) is given by Equation 2.15

$$T_{Ai} = 0 \,, \qquad \text{for } i=1,2,\ldots,14$$

$$T_{Ai}(t) = \pi l_i \rho b^2 U^2 \{\frac{1}{2b}\phi_{ni}\ddot{q}(t) - \phi_{ti}[\frac{3}{8}\ddot{g}(t) + \dot{g}(t)]\} \,, \qquad \text{for } i=15,16,17$$

(3.14)

The inertial moment comes from two sources, one is the rigid body rotation (the step change of angle of attack) of the test rig, the other is due to the fact that the centroids of masses 13 through 17 does not coincide with the pitch axis, as such the normal acceleration of each mass produce an inertial moment about the pitch axis. Hence,

$$T_{Ii} = 0\,, \qquad \text{for } i=1,2, \quad 12$$

$$T_{Ii}(t) = m_i r_i \phi_{ni} \ddot{q}(t) - J_i \ddot{p}(t)\,, \qquad \text{for } i=13,14, \quad 17 \tag{3.15}$$

where J_i is the mass moment of inertia about pitch axis of element i.

The aeroelastic forces and moments have been formulated in terms of the two unknown generalized coordinates q and g. The system equations 3.9a and 3.9b may now be written as:

$$M\ddot{q}+K_n q = \{\phi_n\}^T(\{F_R\}+\{F_A\}+\{F_I\}) \tag{3.16a}$$

$$J\ddot{g}+K_t g = \{\phi_t\}^T(\{T_R\}+\{T_A\}+\{T_I\}) \tag{3.16b}$$

where $\{\phi_n\}$ and $\{\phi_t\}$ are fundamental mode shapes of NDOF and TDOF respectively.

3.8 Nondimensionalization

It is preferable to nondimensionalize the system equations 3.16a-b into dimensionless form, where the generalized coordinate q and time t are nondimensionalized with respect to the airfoil semichord b (=3.0 in). The generalized coordinate g, as well as p, are nondimensional by definition.

Multiplying both sides of Equation 3.16a by $(1/\rho U^2 bl)$ where $\rho=0.03613$ lbm/in^3, U=24 in/s, and l=42 in yields:

$$M^*\ddot{q}^*+K_n^*q^* = \{\phi_n\}^T(\{F_R\}^*+\{F_A\}^*+\{F_I\}^*) \qquad (3.17a)$$

Note that now the dot superscript indicates differentiation with respect to nondimensional time t^* where

$$t^* = \frac{Ut}{b}$$

$$M^* = \frac{\{\phi_n\}^T[M]\{\phi_n\}}{\rho b^2 l}$$

$$q^* = \frac{q}{b}$$

$$K_n^* = \frac{\{\phi_n\}^T[K_n]\{\phi_n\}}{\rho U^2 l}$$

$$F^*_{Ri} = 0 , \qquad \text{for } i = 1,2,\ldots,14$$

$$F^*_{Ri} = \frac{\pi}{3}\{\frac{1}{2}\ddot{p}+\dot{p}+2\int_0^{t^*} \Gamma(t^*-\tau^*)[\ddot{p}(\tau^*)+\dot{p}(\tau^*)]d\tau^*\} , \qquad \text{for } i = 15,16,17$$

$$F^*_{Ai} = 0 , \qquad \text{for } i = 1,2,\ldots,17$$

$$F^*_{Ai} = \frac{\pi}{3}[\phi_{ti}(\frac{1}{2}\ddot{g}+\dot{g})-\phi_{ni}\ddot{q}^*]+\frac{2\pi}{3}\int_0^{t^*} \Gamma(t^*-\tau^*)[\phi_{ti}(\ddot{g}+\dot{g})-\phi_{ni}\ddot{q}^*]d\tau^* ,$$

for i =15,16,17

$$F^*_{Ii} = 0 ,$$ for i =1,2,...,12

$$F^*_{Ii} = \frac{m_i r_i}{\rho b^3 l}[\phi_{ti}\ddot{g}(t^*)+\ddot{p}(t^*)] ,$$ for i =13,14,...,17

Multiply both sides of Equation 3.16b by $(1/\rho U^2 b^2 l)$

$$J^*\ddot{g}+K_t^*g = \{\phi_t\}^T(\{T_R\}^*+\{T_A\}^*+\{T_I\}^*) \tag{3.17b}$$

where

$$J^* = \frac{\{\phi_t\}^T[J]\{\phi_t\}}{\rho b^4 l}$$

$$K_t^* = \frac{\{\phi_t\}^T[K_t]\{\phi_t\}}{\rho U^2 b^2 l}$$

$$T^*_{Ri} = 0 ,$$ for i =1,2,...,14

$$T^*_{Ri} = -\frac{\pi}{3}(\frac{3}{8}\ddot{p}+\dot{p}) ,$$ for i =15,16,17

$$T^*_{Ai} = 0 ,$$ for i =1,2,...,14

$$T^*_{Ai} = \frac{\pi}{3}[\frac{1}{2}\phi_{ni}\ddot{q}^* - \phi_{ti}(\frac{3}{8}\ddot{g}+\dot{g})] \quad , \qquad \text{for } i = 15,16,17$$

$$T^*_{Ii} = 0 \quad , \qquad \text{for } i = 1,2, \quad ,12$$

$$T^*_{Ii} = \frac{m_i r_i}{rb^3 l}\phi_{ni}\ddot{q}^* - \frac{J_i}{\rho b^4 l}\ddot{p} \quad , \qquad \text{for } i = 13,14,\ldots,17$$

Equations 3.17a-b are nondimensional form of system equations which will be solved for nondimensionalized general coordinates q^* and g subject to a prescribed input step change of attack angle p. Note that the superscript * which indicates the nondimensional form of variables will be omitted for brevity in later discussions.

3.9 Input Step

The ideal instantaneous step change of attack angle can be expressed by

$$p(t) = \Delta\alpha u(t-0) \qquad (3.18)$$

where $\Delta\alpha$ is the step amplitude and u is unit step function.

Differentiate (3.18) with respect to t

$$\dot{p}(t) = \Delta\alpha\delta(t-0) \qquad (3.19)$$

where δ is Dirac delta function.

Differentiate (3.19) with respect to t again

$$\ddot{p}(t) = \Delta\alpha\dot{\delta}(t-0) \tag{3.20}$$

where $\dot{\delta}$ is time derivative of delta function.

3.10 Solution of System Equations

The Laplace transform method is used to solve the system equations for a step change in attack angle with an amplitude $\Delta\alpha = 1^o$ ($\pi/180$ radian). Before Laplace transformation is performed, all the coefficients in system equations are calculated. Rearranging the equations yields:

$$1.8526\ddot{q}+9.662q-1.192\ddot{g}-2.006\dot{g}=1.192\ddot{p}+2.063\dot{p}+4.125\int_0^t \Gamma(t-\tau)(\ddot{p}+\dot{p})d\tau$$
$$+4.132\int_0^t \Gamma(t-\tau)(\ddot{g}+\dot{g})d\tau-3.186\int_0^t \Gamma(t-\tau)\ddot{q}d\tau \tag{3.21a}$$

$$1.192\ddot{q}-1.4752\ddot{g}-3.142\dot{g}-1749g=1.518\ddot{p}+3.151\dot{p} \tag{3.21b}$$

Substituting Equations 3.19-20 into above and rearranging yields:

$$1.8526\ddot{q}-1.192\ddot{g}-2.006\dot{g}+9.662g+3.186\int_0^t \Gamma(t-\tau)\ddot{q}d\tau-4.132\int_0^t \Gamma(t-\tau)(\ddot{g}+\dot{g})d\tau$$

$$=0.021\dot{\delta}(t)+0.036\delta(t)+0.072\int_0^t \Gamma(t-\tau)[\dot{\delta}(t)+\delta(t)]d\tau \tag{3.22a}$$

$$1.192\ddot{q}-1.475\ddot{g}-3.142\dot{g}-1749g=0.0265\delta'(t)+0.055\delta(t) \tag{3.22b}$$

Note that $\Gamma(t-\tau)$ is Wagner function given by Equation 2.5.

Taking Laplace transformation of Equations 3.22a-b yields

$$(1.8526s^2+3.1856s - \frac{0.5256s^2}{s+0.0455} - \frac{1.131s^2}{s+0.3} + 9.662)Q -$$

$$(1.1924s^2+6.198s+4.132 - \frac{0.682s(s+1)}{s+0.0455} - \frac{1.467s(s+1)}{s+0.3})G$$

$$= 0.021s+0.108+\frac{0.072}{s} - \frac{0.0119(s+1)}{s+0.0455} - \frac{0.0256(s+1)}{s+0.3} \tag{3.23a}$$

$$1.192s^2Q-(1.4752s^2+3.142s+1749)G = 0.0265s+0.055 \tag{3.23b}$$

where s is the Laplace variable, Q(s) and G(s) are the Laplace transform of q(t) and g(t).

The commercial code MATHEMATICA [17] is used to solve the above algebraic equations symbolically. The solutions of Q(s) and G(s), which are given in Appendix B, are quotients in the form of a sixth order polynomial in s divided by a seventh order polynomial in s.

The quotients are decomposed into partial fractions by MATHEMATICA in order to perform the inverse Laplace transform.

The procedures of the partial fraction decomposition are listed in Appendix C. The inverse Laplace transform is then performed by hand using any mathematical handbook (Appendix D). The solutions for the generalized coordinates in the nondimensional time domain are in the form of:

$$A-Be^{-bt}-Ce^{-ct}+e^{-dt}[D\sin(\omega_1 t)+E\cos(\omega_1 t)]+e^{-ft}[F\sin(\omega_2 t)+G\cos(\omega_2 t)]$$

where t is in semichords and:

$b = 0.29$

$c = 0.0454$

$d = 0.42$

$f = 0.825$

$\omega_1 = 2.29$

$\omega_2 = 49.75$

Note that ω_1 and ω_2 are reduced frequencies which are based on semichord ($\omega b/U$), where ω_1 is associated with the NDOF and ω_2 with the TDOF.

The values of the other constants for each of the nondimensional generalized coordinates are given in the following table.

Table 1. Constants in the Generalized Coordinate Solutions for an Instantaneous Step Input.

Constants	q(t)	g(t)
A	9.73E-3	0.0
B	-2.59E-3	-1.33E-7
C	-1.57E-3	-1.63E-9
D	1.77E-2	-5.10E-5
E	9.25E-3	-5.50E-5
F	-1.04E-3	-3.79E-4
G	-1.55E-2	-2.40E-2

Chapter Four

Results and Discussion

4.1 Sensible Force at the Load Cell

The purpose of this exercise is to determine the aeroelastic effects on the output of the strain gauge load cell. In the experiments, point loads are applied on the midspan of submerged portion of the airfoil (centroid of element 16) to calibrate the strain gauge bridge. The output of the strain gauge is interpreted ideally as that due to the moment exerted by the aerodynamic normal force acting on the same point. In reality, however, the strain gauge output is determined only by the load beam curvature at the cell. This curvature is due not to aerodynamic loading alone, but rather the total aeroelastic structural response.

In elementary beam theory, the moment and beam curvature are related by

$$T(x,t)=EI\frac{d^2V_n(x,t)}{dx^2} \tag{4.1}$$

where $V_n(x,t)$ is the deflection of the beam and x is measured along the span. Since the deflection of the structure is known as a function of time from the results of last chapter, the second derivative in Equation 4.1 (beam curvature) at the load cell (centroid of element 7) can be determined by using a numerical difference method. The method used here is five point Richardson's extrapolation method [18]. The normal force, N, acting at the midspan of the submerged portion of airfoil can then be determined for the purpose of comparison with experimental normal force data. These results are presented in the form of normal force coefficient defined as

$$C_N = C_{N_o} + \frac{N}{\rho U^2 b l} \tag{4.2}$$

where C_{N_0} is normal force at the origin of the motion, and ρ, U, b, L are as described before.

4.2 Results and Discussion

4.2.1 Generalize Coordinates for an Instantaneous Step

The close form solutions of the generalized coordinates have been found in Chapter 3 for a unit step of amplitude $\Delta\alpha = +1^\circ$ at a step onset angle of zero. Figure 4.1a shows the result for the nondimensional NDOF coordinate, q(t), based on semichord. Two vibration frequencies can be observed from the figure. The low frequency is due to direct aeroelastic reaction in the NDOF, while the high frequency oscillation comes from the coupling with the TDOF. Most of the oscillatory response has decayed beyond 3 semichords of travel after the step onset. The steady state value of q(t) determines the steady state normal force via Equation (4.1). As shown below, the steady state value of q(t) yields the correct steady normal force.

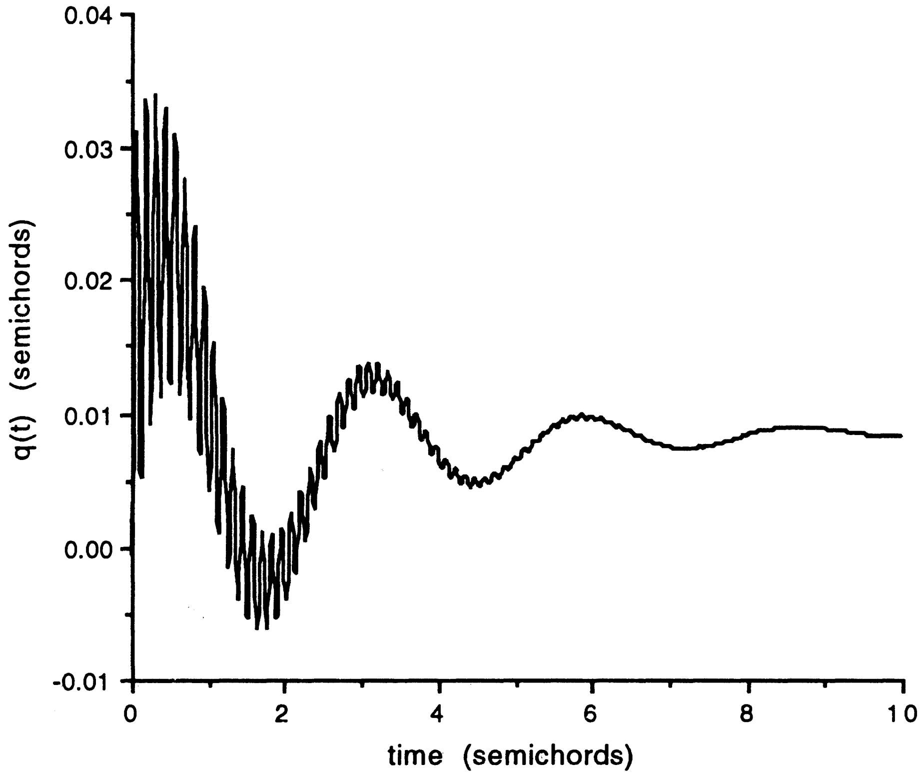

Figure 4.1a Result of NDOF Generalized Corrdinate

Figure 4.1b shows the result for the nondimensional TDOF coordinate, g(t). The magnitude of the TDOF oscillation is very small compared with that of the NDOF oscillation. A steady state value at zero is observed. This result agrees with the fact that the resultant force of the steady state normal force acts at the quarter chord which is coincident with the pitch axis of the present test rig and thus it gives zero moment.

4.2.2 Comparison with Theoretical Normal Force Response

Figure 4.2 is a comparison of the theoretical response of Equation 1.1 (zero onset angle of attack) with the aeroelastic sensible force of the present analysis. Significant aeroelastic effects shortly after the step onset due to the direct NDOF response (low frequency) and TDOF response (high frequency) can be observed. The aeroelastic response of present study gives measurable differences with the theoretical response for a rigid 2D airfoil. The steady state aeroelastic response is a little larger than the steady state theoretical response. The difference may be due to roundoff errors. The capability of predicting the total structural response gives rise to the interesting possibility for developing a rational to correct experimental strain gauge data accordingly and extract therefrom the aerodynamic component of interest.

4.2.3 Comparison with Experiment Data

Figure 4.3a shows a comparison of the result of present analysis with the experimental data taken in the Ohio University tow tank. These data are same as in Figure 1.3b. The step onset angle is 2.09 deg. and the step amplitude is 1.3 deg. as shown in Figure 1.3a.

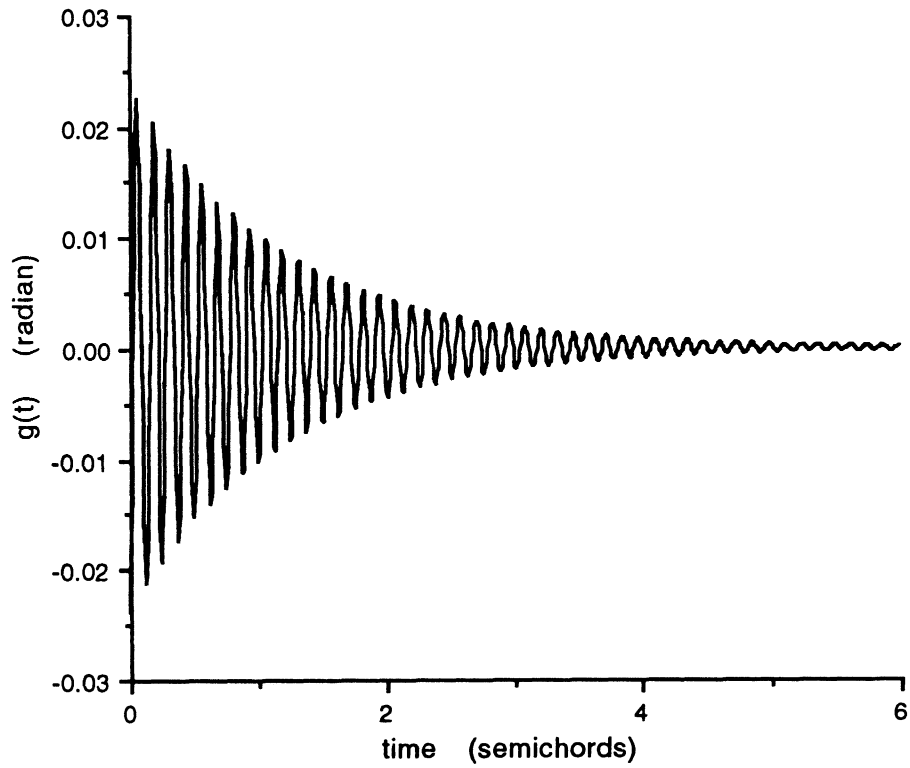

Figure 4.1b Result of TDOF Generalized Coordinate

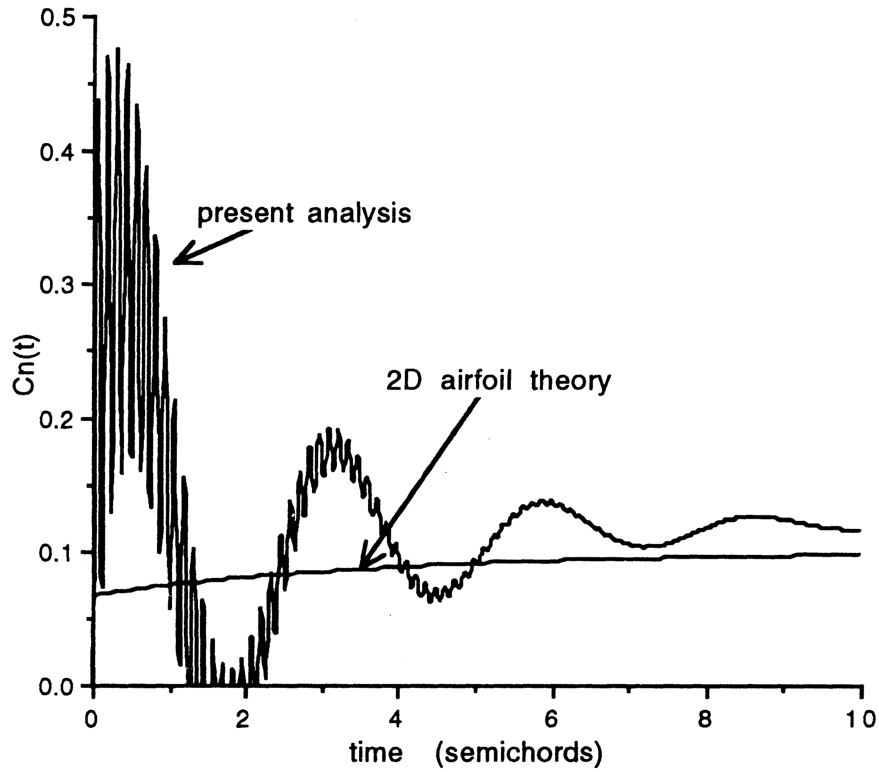

Figure 4.2 Comparison of Present Aeroelastic Response with Wagner Function (for step onset angle = 0 deg, step = 1 deg)

C_{N_0} can be calculated by Equation 2.1 which gives the result of 0.22 for step onset 2.09 deg. Static tests in O.U. tow tank gave a normal force close to this value. The comparison of the experimental data with the theoretical response has been given in Figure 1.3b. In order to compare with the test data, the present analytical response has been multiplied by a factor of 1.3 by assuming that the response is linearly related to step amplitude. In Figure 4.3a, there is sufficient agreement between the analytical result and the test data to conclude that the rise in the strain gauge data shortly after the step, followed by an underdamped oscillation is due to aeroelasticity. Such a conclusion is not a priori possible since such behavior could very well arise from aerodynamics alone, particularly when considering that the noncirculatory loading at the step origin is theoretically large and positive. Figure 4.3b and 4.3c are magnified view of Figure 4.3a. In Figure 4.3b, the experiment data indicate a lower frequency of vibration than the analysis below 1.0 semichord. This might be expected since the actual structure is less stiff than the analytical model due to deformations in the I-beams, gear box, etc. Also, this frequency may be associated with a higher NDOF mode not considered here. The high frequency oscillations in the experiment data appear to damp out faster than the analysis which may be due to the fact that no structural damping is put into the analytical model.

4.3 Reduced Frequency and Apparent Mass

Apparent mass and apparent inertia arise from second order noncirculatory terms in the aerodynamic normal force and moment

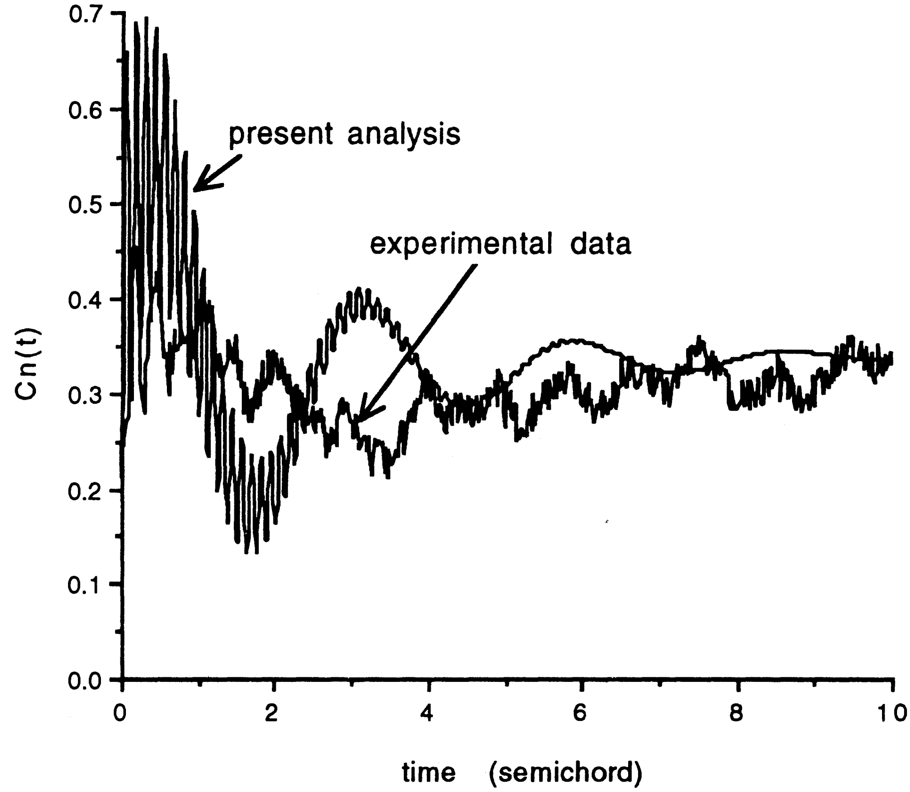

Figure 4.3a Comparison of present analysis with experimental data (step onset angle = 2 deg, step = 1.3 deg)

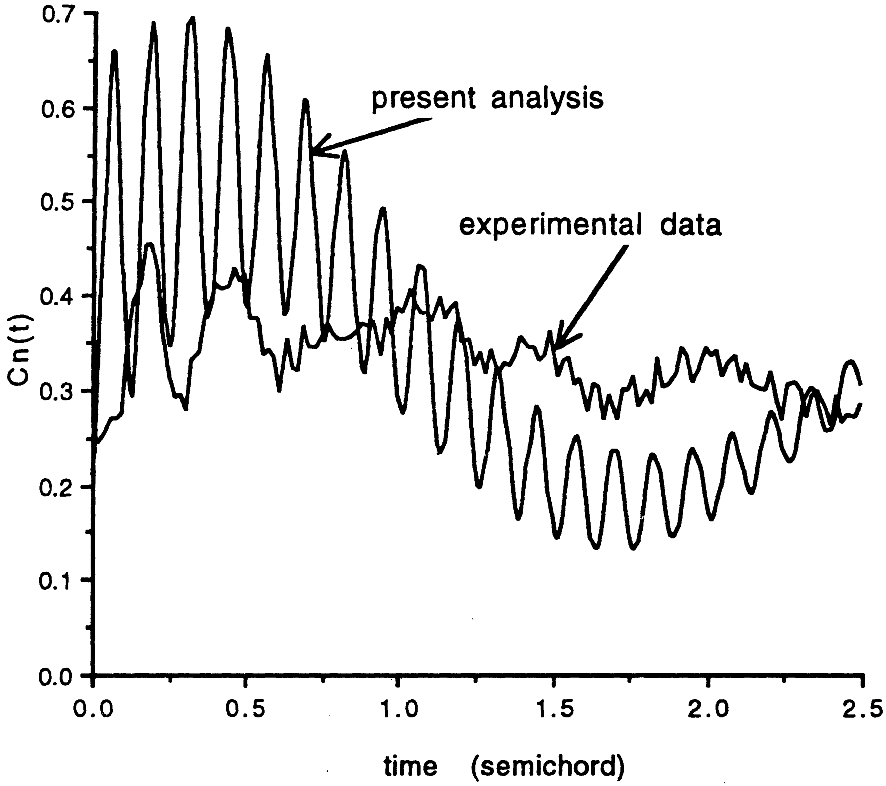

Figure 4.3b Magnified view of figure 4.3a

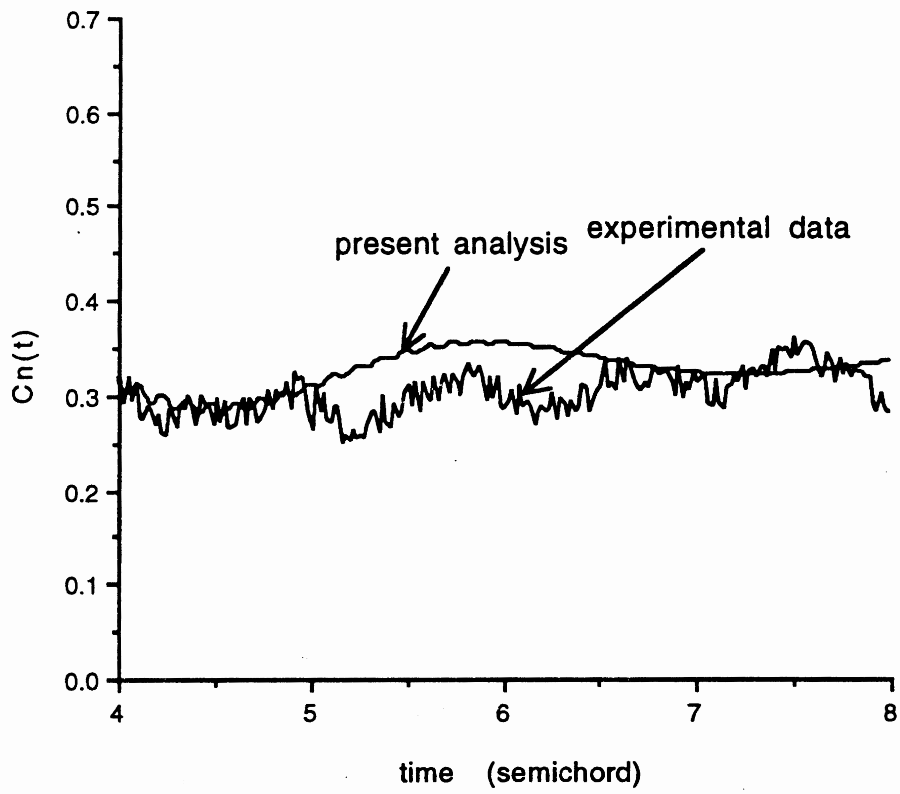

Figure 4.3c Magnified view of Figure 4.3a

representations. These terms introduce sufficient "added" mass and inertia to cause a significant shift in the vibrational frequencies of the structure. More specifically, the NDOF fundamental frequency is reduced from 7.74 hz (with no water in the tank) to 2.92 hz, and the TDOF fundamental frequency is reduced from 97.38 hz to 63.34 hz. It may be possible to use Fourier analysis to provide an indirect measurement of apparent mass. This may be a useful technique in the nonlinear aerodynamics problem where, to the author's knowledge, the effect of apparent mass has not been widely studied.

4.4 Limitations and Further Study

The problem of finding the dynamic response to a unit step in angle of attack has been solved using a mode superposition model. Actually this model is sufficiently general to simulate any prescribed motion given that the angle of attack is small and the fluid is incompressible. The limitation is due to the fact that the indicial response given by Wagner's function is only valid for small angles of attack and incompressible flow.

For large angle of attack, no functional forms of the indicial response are currently available. Experimental data of indicial response may be used in the convolution integral representation of aerodynamic response.

The results of present study may be improved by incorporating actual stiffness matrix data measured on the test rig. It is expected that the actual rig is less stiff than the theoretical values derived here in.

Chapter Five

Conclusions

The present work provides a mathematical model for studying the aeroelastic effects in experimental measurement of the indicial response of airfoil. Closed form solutions have been found for a testing undergoing a small step change in angle of attack. The results have shown fair agreement with experimental data. Evident aeroelastic effects have been shown when comparing present analytical result with Wagner's function. The ability of this model to predict the structural response gives rise to the interesting possibility for developing a method to correct experimental strain gauge data accordingly and extract therefrom the aerodynamic component of interest. Additional experiments are needed for direct measurement of the system structural properties such as flexibility, natural frequencies, and material properties for incorporating into the analysis.

Appendix A

System Matrices

The 17x17 mass matrix [M] and the 13x13 polar mass moment of inertia matrix are diagonal matrices listed as follows:

M_{ii} = 2.2122, .1425, .9794, .9794, .06632, .06632, .06632, .06632, .06632, 1.0754, 1.0754, .4313, 3.1785, .3596, 2.2372, 2.2372, 2.2372 (lbm)

for i= 1, 2, ..., 17

Jii = 2.20, .02784, .4897, .4897, .01338, .01338, .01338, .01338, .01338, .5378, .5378, .1468, 35.58 ($lbm\text{-}in^2$)

for i= 1, 2, ..., 17

Virtual work method is used to calculate the NDOF flexibility matrix. The principle of virtual work for deformable bodies is stated as [16]:

If a deformable body is in equilibrium under a virtual Q-force system and remains in equilibrium while it is subjected to a small and compatible deformation, then the external virtual work done by the external Q forces is equal to the internal virtual work of deformation done by the internal Q stresses.

Let us take an example to explain how to apply the above principle to the flexibility calculation of beams. Consider a cantilever beam shown in Figure A.1. According to the definition of flexibility influence coefficient (that is $A_{ni,j}$ is equal to the deflection of point i due to a unit force applied at point j), a unit force $P_j=1$ lbf is applied at point j. In order to calculate the

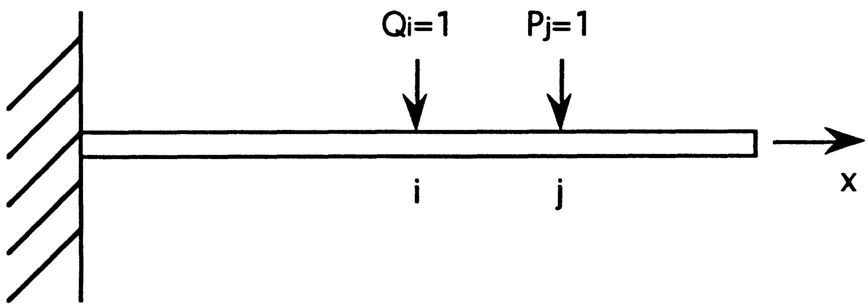

Figure A.1 A Cantilever Beam

deflection of point i caused by force$_j$, we assume a unit virtual force $Q_i=1$ lbf acting at point i. The principle of virtual work as applied to this case will be simply

$$Q_i \, A_{ni,j} = \int M_Q M_P \frac{dx}{EI} \tag{A.1}$$

where M_Q and M_P are the moments due to load Q and P respectively, E is Young's modulus of elasticity, I is the moment of inertia of cross-sectional area of the beam. Thus the beam deflection problem become the evaluation of the integration on the right-hand side of Equation (A.1).

Before the integration of the right-hand side can be accomplished, both M_Q and M_P must first be expressed as functions of x. It is necessary to separate the integration for the entire beam into the sum of several integrals, one for each of several portions of the beam. The integration must be broken at points where there is a change in the functions representing MQ, MP, or E, I in terms of x.

The results of NDOF flexibility matrix [AN] which is a 17x17 matrix are listed below.

[AN] = [1.67 3.816 6.117 9.47 11.61 12.53 13.45 14.37 15.29 17.59 21.27 24.2 26.6 29.09 37.64 52.37 67.09;

3.816 8.948 14.85 23.45 28.93 31.29 33.65 36.01 38.37 44.27 53.71 61.22 67.37 73.78 95.7 133.5 171.2;

6.117 14.85 30.36 53.89 68.89 75.34 81.8 88.26 94.72 110.9 136.7 157.2 174.1 191.6 251.6 354.9 458.3;

9.47 23.45 53.89 104 136.5 150.6 164.6 178.6 192.6 227.7 283.4 364.9 403 533.2 757.5 981.9;

11.61 28.93 68.89 136.5 182 201.7 221.5 241.2 261 310.4 389.3 452.1 503.6 557.2 740.6 1057 1372;

12.53 31.29 75.34 150.6 201.7 224.5 247.4 270.3 293.2 350.4 441.9 514.6 574.3 636.4 848.9 1215 1581;

13.45 33.65 81.8 164.6 221.5 247.4 273.9 300.5 327.2 393.8 500.3 585 654.4 726.7 974.1 1400 1826;

14.37 36.01 88.26 178.6 241.2 270.3 300.5 333.3 364.3 441.8 565.9 664.4 745.3 819.5 111701613 2110;

15.29 38.37 94.72 192.6 261 293.2 327.2 364.3 398.4 488.4 632.4 746.8 840.6 938.3 1273 1849 2424;

17.59 44.27 110.9 227.7 310.4 350.4 393.8 441.8 488.4 613.4 814.1 973.5 1104 1241 17.6 2509 3312;

21.27 53.71 136.7 283.8 389.3 441.9 500.3 565.9 632.4 814.1 1111 1348 1542 1745 2437 3629 4822;

24.2 61.22 157.2 328.4 452.1 514.6 585 664.4 746.8 973.5 1348 1650 1899 2158 3043 4569 6095;

26.6 67.37 174.0 364.9 503.6 574.9 654.4 745.3 840.6 1104
1542 1899 2196 2505 3564 5388 7212;
29.09 73.78 191.6 403 557.2 636.4 726.7 829.5 938.3 1241
1745 2158 2505 2868 4115 6265 8414;
37.64 95.7 251.6 533.2 740.6 848.9 974.1 1117 1273 1706
2437 3043 3564 4115 6290 10219 14148;
52.37 133.5354.9 757.5 1057 1215 1400 1614 1849 2509
3629 4569 5388 6265 10219 19257 28839;
67.09 171.2 458.3 981.9 1372 1581 1826 2110 2424 3312
4822 6095 7212 8414 14148 28839 46791] (in/lbf)

The TDOF flexibility matrix of the system [AT] is calculated from elementary torsional shaft theory. Consider a circular shaft as shown in Figure A.2.

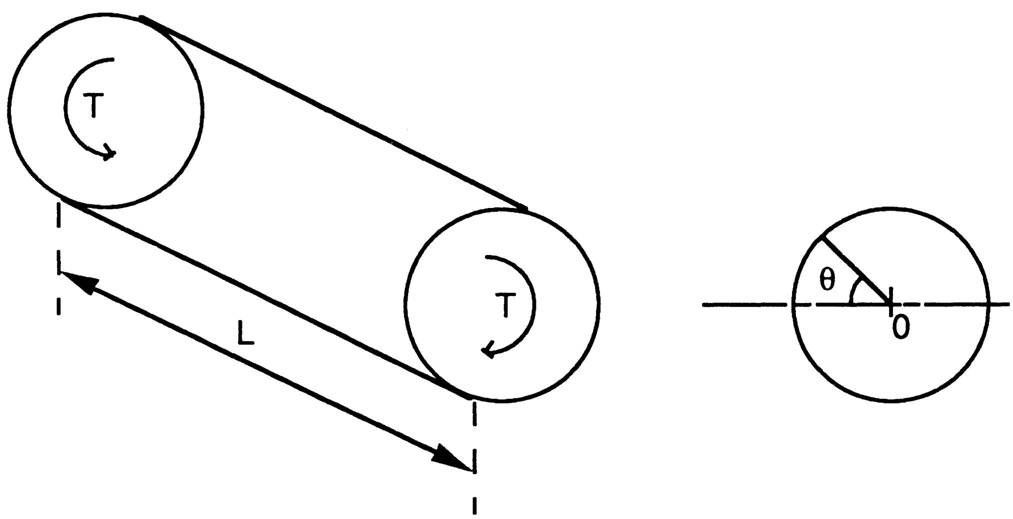

Figure A.2 Deformation of circular shaft

For circular shafts, the torsional angle θ is related with torque T by

$$\theta = \frac{TL}{JG} \tag{A.2}$$

where T is applied torque, L is the length of shaft, J is the polar moment of inertia of the cross-section, G is modulus of rigidity.

For rectangular shafts, the torsional angle θ is related with torque T by

$$\theta = \frac{TL}{\beta a^3 b G} \tag{A.3}$$

where a and b are the lengths of the short and long sides of the rectangle. The numerical factor β can be obtained from any mechanical engineering handbook.

[AT] = [0.8823 0.8823 0.8823 0.8823 0.8823 0.8823 0.8823 0.8823
0.8823 0.8823 0.8823 0.8823 0.8823 ;
0.8823 1.5783 1.5783 1.5783 1.5783 1.5783 1.5783 1.5783
1.5783 1.5783 1.5783 1.5783 1.5783;
0.8823 1.5783 2.4970 2.4970 2.4970 2.4970 2.4970 2.4970
2.4970 2.4970 2.4970 2.4970 2.4970;
0.8823 1.5783 2.4970 3.0310 3.0310 3.0310 3.0310 3.0310
3.0310 3.0310 3.0310 3.0310 3.0310;
0.8823 1.5783 2.4970 3.0310 5.5720 5.5720 5.5720 5.5720
5.5720 5.5720 5.5720 5.5720 5.5720;

0.8823 1.5783 2.4970 3.0310 5.5720 10.120 10.120 10.120
10.120 10.120 10.120 10.120 10.120;
0.8823 1.5783 2.4970 3.0310 5.5720 10.120 14.670 14.670
14.670 14.670 14.670 14.670 14.670;
0.8823 1.5783 2.4970 3.0310 5.5720 10.120 14.670 19.220
19.220 19.220 19.220 19.220 19.220;
0.8823 1.5783 2.4970 3.0310 5.5720 10.120 14.670 19.220
23.760 23.760 23.760 23.760 23.760;
0.8823 1.5783 2.4970 3.0310 5.5720 10.120 14.670 19.220
23.760 26.330 26.330 26.330 26.330;
0.8823 1.5783 2.4970 3.0310 5.5720 10.120 14.670 19.220
23.760 26.330 26.920 26.920 26.920;
0.8823 1.5783 2.4970 3.0310 5.5720 10.120 14.670 19.220
23.760 26.330 26.920 27.580 27.580;
0.8823 1.5783 2.4970 3.0310 5.5720 10.120 14.670 19.220
23.760 26.330 26.920 27.580 27.970] (1/lbf-in)

Appendix B

Solving of the System Equation

The system equations 3.23a-b are solved symbolically by Mathematica as follows where qone and qtwo are Q(s) and G(s) respectively as in Equations 3.23.

$\text{Solve}[\{(1.8528s^2+3.186s-.526s^2/(s+.0455)$

$(1.13s^2/(s+.3))+9.662)*\text{qone}-(1.192s^2+6.198s+4.132-$

$(.682s(s+1)/(s+.0455))-(1.467s(s+1)/(s+.3)))*\text{qtwo}==$

$.021s+.108+(.072/s)-(.0119(s+1)/(s+.0455))-.0256(s+1)/(s+.3),$

$1.192s\text{^}2*\text{qone}-(1.4752s\text{^}2+3.142s+1749)*\text{qtwo}==$

$.0265s+.055\},\{\text{qone},\text{qtwo}\}]$

The solutions are

$\text{qone} \to (1.7189 + 37.805s + 117.82s^2 + 135.99s^3 + 36.725s^4 -$
$0.0030852s^5 - 0.0006088s^6)/(230.67s + 5915.0s^2 + 18513s^3$
$+ 3832.3s^4 + 3258.4s^5 + 3.7056s^6 + 1.3124s^7)$

$\text{qtwo} \to -(0.0072537s + 0.18832s^2 + 0.64569s^3 + 0.3194s^4 +$
$0.066728s^5 + 0.024067s^6)/(230.67s + 5915.0s^2 + 18513s^3$
$+ 3832.3s^4 + 3258.4s^5 + 3.7056s^6 + 1.3124s^7)$

Appendix C

Partial Fraction of the Solution

The procedures of decomposing the quotient solution into partial fraction forms by Mathematica are listed as follows.

1. Finding the roots of the denominator (note that Q(s) and G(s) have the same denominator) using Roots command.

$$\text{Roots}[230.669 + 5915.03s + 18513.1s^2 + 3832.33s^3 + 3258.36s^4 +3.706s^5+1.312s^6 == 0, s]$$

The roots are found to be

s == -0.824723 - 49.7513 I
s == -0.824723 + 49.7513 I
s == -0.420152 - 2.28624 I
s == -0.420152 + 2.28624 I
s == -0.28956
s == -0.045386

The root 0 is obvious, thus there are four complex roots and three real roots for the denominator.

2. Partial fraction of Q(s).

Assume that

```
Q(s) = a/(s+.29)+b/(s+.0454)+(cs+d)/((s+.825)^2+49.75^2)
+(es+f)/((s+.42)^2+2.29^2)+g/s                                (B.1)
```

Multiply both sides of Equation B.1 by the denominator of Q(s) using the Expand command in Mathematica. The right-hand side of (B.1) becomes

```
RHS of (B.1) = Expand[a*s*(s+0.0454)*((s+0.825)^2+49.75^2)*
    ((s+0.42)^2+2.29^2)+b*s*(s+0.29)*((s+0.825)^2+49.75^2)*
    ((s+0.42)^2+2.29^2)+(c*s+d)*s*(s+0.29)*(s+0.0454)*
    ((s+0.42)^2+2.29^2)+(e*s+f)*s*(s+0.29)*(s+0.0454)*
    ((s+0.825)^2+49.75^2)+g*(s+0.29)*(s+0.0454)*((s+0.825)^2
    +49.75^2)((s+0.42)^2+2.29^2)]
    = 176.6846340089169*g + 609.2573586514376*a*s +
      3891.732026628125*b*s + 0.07136630300000002*d*s +
      32.59563398375001*f*s + 4528.487472225863*g*s +
      13514.5865985325*a*s^2 + 14025.4503435625*b*s^2 +
      0.07136630300000002*c*s^2 + 1.82909514*d*s^2 +
      32.59563398375001*e*s^2 + 830.385968025*f*s^2 +
      14152.95658139525*g*s^2 + 2201.275802975*a*s^3 +
      2808.50744125*b*s^3 + 1.82909514*c*s^3 +
      5.715402*d*s^3 + 830.385968025*e*s^3 +
      2476.309701*f*s^3 + 2921.247977564999*g*s^3 +
      2482.662671*a*s^4 + 2483.271725*b*s^4 + 5.715402*c*s^4
      + 1.1754*d*s^4 + 2476.309701*e*s^4 + 1.9854*f*s^4 +
      2483.397937*g*s^4 + 2.5354*a*s^5 + 2.78*b*s^5 +
      1.1754*c*s^5 + d*s^5 + 1.9854*e*s^5 + f*s^5 +
      2.8254*g*s^5 + a*s^6 + b*s^6 + c*s^6 + e*s^6 + g*s^6
```

At this point, let the coefficients with the same power of s of both sides be equal and then use the command Solve to solve the linear algebraic simultaneous equations.

```
Solve[{ 176.685*g== 1.7189,
      609.257*a + 3891.7*b + 0.071366*d +
      32.596*f+4528.5*g==37.805,
      13515*a+ 14025*b+ 0.071366*c+ 1.8291*d+
      32.596*e+ 830.39*f+14153*g == 117.822,
      2201.3*a+2808.5*b+ 1.8291*c+5.7154*d+ 830.39*e+
      2476.3*f+ 2921.2*g == 135.992,
      2482.7*a+ 2483.3*b+ 5.7154*c+1.1754*d+ 2476.3*e+
      1.9854*f+ 2483.4*g == 36.7248,
      2.5354*a+ 2.78*b +1.1754*c+ d+ 1.9854*e+ f+
      2.8254*g == -0.00308524,
      a+ b+ c+ e+ g == -0.0006088},{a,b,c,d,e,f,g}]
```

The coefficients a to g for Q(s) are found to be

```
a -> -0.00259014,
b -> -0.00157293,
c -> -0.0154531,
d -> -0.0644672,
e -> 0.00927874,
f -> 0.0445761,
g -> 0.00972861
```

3. <u>Partial fraction of G(s):</u>

Assume that

```
G(s) = a/(s+.29)+b/(s+.0454)+(cs+d)/((s+.825)^2+49.75^2)
       +(es+f)/((s+.42)^2+2.29^2)+g/s                        (B.2)
```

Using similar procedures as step two, we can find the coefficients for G(s).

```
Solve[{ 176.685*g== 0,
    609.257*a+3891.7*b+0.071366*d+32.596*f+4528.5*g==
    -.0072538,
    13515*a+ 14025*b+ 0.071366*c+ 1.8291*d+ 32.596*e+
    830.39*f+14153*g == -.18832,
    2201.3*a+2808.5*b+ 1.8291*c+5.7154*d+ 830.39*e+
    2476.3*f+ 2921.2*g == -.645686,
    2482.7*a+ 2483.3*b+ 5.7154*c+1.1754*d+ 2476.3*e+
    1.9854*f+2483.4*g == -.319397,
    2.5354*a+ 2.78*b +1.1754*c+ d+ 1.9854*e+ f+2.8254*g ==
    -0.0667282,
    a+ b+ c+ e+ g == -0.0240672},{a,b,c,d,e,f,g}]
```

a -> $-1.33020442739471 3*10^{-7}$

b -> $-1.633259815288864*10^{-9}$

c -> -0.0240119082133844

d -> -0.03825866099566486

e -> -0.00005515713291303789

f -> -0.0001360913181447368

g -> $-7.027684604910015*10^{-18}$

Appendix D

Inverse Laplace Transformation

The partial fraction forms of Q(s) and G(s) are:

$$Q(s) = \frac{0.00973}{s} - \frac{0.00259}{s+0.29} - \frac{0.00157}{s+0.0454} - \frac{0.0155s+0.0645}{(s+0.825)^2+49.75^2}$$

$$+ \frac{0.00928s+0.0446}{(s+0.42)^2+2.29^2}$$

$$G(s) = -\frac{1.13\times10^{-7}}{s+0.29} - \frac{1.633\times10^{-9}}{s+0.0454} - \frac{0.024s+0.0383}{(s+0.825)^2+49.75^2}$$

$$- \frac{0.000055s+0.00014}{(s+0.42)^2+2.29^2}$$

Taking inverse Laplace transformation of above two equations, noting that,

$$L^{-1}\left\{ \frac{s+d}{(s-a)^2+w^2} \right\} = Ae^{at}\sin(wt+\alpha)$$

where

$$A = \frac{1}{w}[(a+d)^2+w^2]^{0.5}$$

$$\alpha = \arctan\frac{w}{a+d}$$

we get

$$q(t) = 0.00973 - 0.00259Exp(-0.29t) - 0.00157\ Exp(-0.0454t) + 0.02Exp(-0.42t)\sin(2.29t+0.481) - 0.0155Exp(-0.825t)\sin(49.75t+1.504)$$

$$g(t) = -\ 0.000000133Exp(-0.29t) - 0.00000000163Exp(-0.0454t) - 0.000075Exp(-0.42t)\sin(2.29t+0.823) - 0.\ \ 024Exp(-0.825t)\sin(49.75t+1.56)$$

References

1. Graham, G. M., Islam, M. and Jenkins, J. E., "Nonlinear Normal Force Indicial Responses for 2-D Airfoil," AIAA Atmospheric Flight Mechanics Conference, AIAA-91-2866-CP New Orleans, La., August 1991.

2. Tobak, M. and Schiff, L. B., "Aerodynamic Mathematical Modeling-Basic Concepts," AGARD Lecture Series No.114, Paper 1, March 1981.

3. Bisplinghoff, R. L. and Ashley, H., *Principles of Aeroelasticity*, Dover Publications Inc., New York, 1962.

4. Graham, G. M., Fang, K. C., and Islam, M., "Nonlinear Normal and Axial Force Indicial Responses for a Two Dimensional Airfoil," final report submitted to AFOSR under Grant AFOSR-89-0502, November 1991.

5. Graham, G.M., "An Experimental Investigation of High Pitch Rate and High Lift Aerodynamics of Unsteady Airfoil," final report submitted to AFOSR under Grant AFOSR-87-0312, March 1989.

6. Islam, M. M., "Nonlinear Normal Force Indicial responses for a 2-D NACA 0015 Airfoil," M.S. thesis, Ohio University, November 1991.

7. Beddoes, T. S., "A Synthesis of Unsteady Aerodynamic Effects including Stall Hysteresis," Vertica, Vol. 1, pp 113-123, 1976.

8. Beddoes, T. S., "Practical Computation of Unsteady Lift," Vertica, Vol. 8, No. 1, pp55-71, 1984.

9. Leishman, J. G., Beddoes, T. S., "A Generalized Model for Airfoil Unsteady Aerodynamic Behavior and Dynamic Stall Using the

Indicial Method" 42nd. Annual Forum of the American Helicopter Society, Washington D. C., June 1986.

10. Wagner, H., "Uber die Entstehung des Dynamischen Auftriesbes bon Tragflugeln," Zeitschrift fur Angewandte Mathematik und Mechanic, Vol. 5, No. 1, Feb. 1925.

11. Fung, Y. C. *An Introduction to the Theory of Aeroelasticity*, Dover Publications, New York, 1969.

12. Kaplan, W. K., *Advanced Calculus*, Addison-Wesley Publishing Co., 2nd ed., pp. 515-521.

13. Currie, I. G.*Fundamental Mechanics of Fluids,* Published by McGraw-Hill, Inc., 1974.

14. Clough, R. W. and Penzien, J., *Dynamics of Structures*, Published by McGraw-Hill, Inc., 1975.

15. Utku, S., Norris, C. H., and Wilbur, J. B., *Elementary Structural Analysis*, Published by McGraw-Hill, Inc., 4th ed..

16. *MATLAB*, The MathWorks, Inc., Cochituate Place, 24 Prime Parkway, Natick, MA 01760.

17. Wolfram, S *METHEMATICA,* Addison-Wesley Publishing Co., 2nd ed., 1991.

18. Burden, R. L., Farres, J. D., and Reynolds, A. C., *Numerical Analysis*, Prindle, Weber & Schmidt Boston, Ma., 1980.